Advanced Drug Delivery Reviews 151–152 (2019) 72–93

Contents lists available at ScienceDirect

Advanced Drug Delivery Reviews

journal homepage: www.elsevier.com/locate/addr

Physical and chemical profiles of nanoparticles for lymphatic targeting

Xiyu Ke [a,b], Gregory P. Howard [a,c], Haoyu Tang [a], Bei Cheng [d], May Tun Saung [e], José L. Santos [f,*], Hai-Quan Mao [a,b,c,g,**]

[a] Institute for NanoBioTechnology, Johns Hopkins University, Baltimore, MD 21218, USA
[b] Department of Materials Science and Engineering, Whiting School of Engineering, Johns Hopkins University, Baltimore, MD 21218, USA
[c] Department of Biomedical Engineering, Johns Hopkins School of Medicine, Baltimore, MD 21205, USA
[d] Department of Radiology, Johns Hopkins University School of Medicine, Baltimore, MD 21205, USA
[e] Department of Oncology, Johns Hopkins University School of Medicine, Baltimore, MD 21205, USA
[f] Dosage Form Design & Development, AstraZeneca, Gaithersburg, MD 20878, USA
[g] Translational Tissue Engineering Center, Johns Hopkins University School of Medicine, Baltimore, MD 21205, USA

ARTICLE INFO

Article history:
Received 18 June 2019
Received in revised form 3 September 2019
Accepted 24 September 2019
Available online 15 October 2019

Keywords:
Nanoparticles
Physicochemical properties
Vaccine
Immunotherapy
Lymph node
Immune cells

ABSTRACT

Nanoparticles (NPs) have been gaining prominence as delivery vehicles for modulating immune responses to improve treatments against cancer and autoimmune diseases, enhancing tissue regeneration capacity, and potentiating vaccination efficacy. Various engineering approaches have been extensively explored to control the NP physical and chemical properties including particle size, shape, surface charge, hydrophobicity, rigidity and surface targeting ligands to modulate immune responses. This review examines a specific set of physical and chemical characteristics of NPs that enable efficient delivery targeted to secondary lymphoid tissues, specifically the lymph nodes and immune cells. A critical analysis of the structure-property-function relationship will facilitate further efforts to engineer new NPs with unique functionalities, identify novel utilities, and improve the clinical translation of NP formulations for immunotherapy.

Contents

* Corrrespondence to: J.L. Santos, Dosage Form Design & Development, AstraZeneca, Gaithersburg, MD 20878, USA.
** Correspondence to: H-Q. Mao, Institute for NanoBioTechnology, Johns Hopkins University, Baltimore, MD 21218, USA.
E-mail addresses: luis.santos1@astrazeneca.com (J.L. Santos), hmao@jhu.edu (H.-Q. Mao).

https://doi.org/10.1016/j.addr.2019.09.005
0169-409X/

1. Introduction

1.1. Vaccines and immunotherapy

The immune system plays a vital role in protecting the human body against pathogens such as bacteria and viruses. The discovery of vaccines has paved the way for modulating the immune system for disease prevention and treatment. Traditional prophylactic vaccines were composed of whole pathogens in live-attenuated or killed/inactivated forms. These vaccines have been effective in preventing a variety of infectious diseases including tetanus, diphtheria, polio, typhoid and chickenpox, but they can be less effective in young and old populations as well as recipients with immunodeficiency, and may even cause severe toxicities due to the risk of virulence reversion [1,2]. Furthermore, effective vaccines are still unavailable for many morbid infectious diseases such as HIV, dengue, chikungunya, Zika, and malaria. To address these challenges, a new generation of well-defined subunit vaccines composed of inactivated proteins, synthetic peptides, or plasmid DNA encoding the specific antigens are being developed [3–5]. Although these vaccines are considered to be safer than traditional whole pathogen vaccines, their widespread applications have been impeded by their low immunogenicity and poor immune memory induction [1]. Currently, commercially available adjuvants include aluminum salts, emulsions (MF59 and AS03), Toll-like receptor (TLR) agonists adsorbed on aluminum (AS04) and combination of immunopotentiators (QS-21 and MPL in AS01), which were developed empirically [6,7]. There is an increasing need to develop new adjuvants to elicit the potency of the next generation of vaccines.

In addition to vaccines, other forms of immunotherapy have drawn increasing attention in the last few decades, particularly in the field of cancer therapy [1,8,9]. Currently available cancer immunotherapy repertoire includes cytokines for modulating the host immune system and antibodies against check-point molecules such as programmed cell death protein 1 (PD-1) and cytotoxic T-lymphocyte-associate protein 4 (CLTA-4) [10]. Despite some agents having shown great promise for the treatment of a subset of cancer patients, there remains a substantial population for whom currently available immunotherapies are ineffective. To improve treatment response, investigators have tried combining different immunotherapy agents. However, such a combinatorial approach may increase the risk of off-target "immune-related adverse events" that manifest as a diverse range of autoimmune diseases. For example, in patients with untreated unresectable stage III or IV tumors, the combination of Nivolumab and Ipilimumab increased the median progression-free survival to 11.5 months compared to 2.9 months with Ipilimumab alone and 6.9 months with Nivolumab alone, respectively. However, the combination also increased Grade 3 or 4 treatment-related adverse events from 16.3% of the patients in the Nivolumab group and 27.3% of those in the Ipilimumab group to 55.0% of those in the combination treatment group [10].

1.2. Lymphatic system

An important target for modulating the immune response *via* prophylactic or therapeutic interventions is the lymphatic system and secondary lymphoid organs, especially the major draining lymph nodes (dLNs). Early characterization of the lymphatics established the lymphatic's main role in reabsorption of fluids and electrolytes lost by Starling forces at the capillary beds [11]. Starling's law states that arterioles, capillaries, and venules contribute to fluid filtration and plasma proteins pulled into the interstitial space [12]. With this understand, the lymphatic system acts as a sewer system that absorbs protein rich exudate and dietary fats, and recycles this filtrate back to the blood by way of the thoracic duct [13]. This view evolved to the lymphatics important role as an antigen "information superhighway" that samples and concentrates upstream inflammatory cues within the dLNs [14]. The dLN structure allows the innate immune response to meet the adaptive immunity and to pass off key information about the foreign invader or state of self, thereby maximizing the likelihood of a productive encounter between an antigen presenting cell (APC) and low-frequency antigen-specific T- or B-cell and initiation of a successful immune response and resolution of infection [14]. Given that the LN is the meeting ground for productive immunological interactions, the lymphatic system is a key target for immunomodulation.

Targeting the LNs *via* the lymphatics for initiation of the immune response has been well explored over the past 15 years. Early work using labeled dextrans and liposomes determined the optimal size and charge characteristics for delivery [15–20]. It was not clear if delivery to a single LN could initiate a systemic immune response or if the response would remain locally. Antigen depots administered by direct intra-LN delivery that retains antigen and adjuvant within the dLN [21] resulted in a systemic response in a tolerogenic vaccine multiple sclerosis (MS) model leading to alleviation of MS symptoms in mice [22]. Memory B- and T-cells have been shown to be preferentially enriched within the dLN and interrogate incoming antigens in the lymph and quickly become activated to clear the infection [23,24]. This highlights not only the importance in targeting the LNs for initiating an immune response but also for boosting an immune response and formation of subsequent memory. Current evidence suggests that memory T- and B-cells are restricted to the dLNs that originate the immune response, leaving many unanswered questions as to the best priming and boosting vaccination regimen and location of prime/boost (*e.g.* same dLN target for prime/boost or different dLN target for prime and boost) that yields the most effective systemic immune response and immune memory formation [25]. Targeting APCs and B−/T-cell memory is key for robust vaccine formulations.

1.3. Nanoparticles (NPs) for immunoengineering

NPs have been increasingly proposed for the delivery of immunomodulatory molecules to improve the potency and reduce the safety concerns raised by vaccines and immunotherapy agents [1,26,27]. For example, the combination therapy using oxaliplatin and NPs loaded plasmid DNA encoding PD-L1 trap fusion protein significantly enhanced the antitumor effect and decreased the "immune-related adverse events" compared to the treatment of oxaliplatin plus anti-PD-L1 antibody in murine orthotopic colorectal, melanoma and breast cancer models [28]. Compared to traditional delivery systems, nanoparticulate systems are more desirable by virtue of their unique properties: (a) NPs can significantly lower the side effects induced by immunomodulatory agents through specific agent delivery to select lymphoid tissues or immune cells; (b) this targeted delivery can enhance the potency of these payloads, reducing the required dose to elicit an effective immune response; (c) NPs can protect and stabilize these immunomodulatory compounds *in vivo*; (d) NPs can enable co-delivery of antigens and immunomodulatory agents simultaneously to the lymphoid tissues and immune cells in a single vehicle, enhancing the activity of these agents; and (e) some NPs may also have intrinsic immunomodulatory properties that can ameliorate the immune response induced by the payloads. Various types of nanoparticular systems have been designed and employed for the delivery of vaccines and immunotherapy agents, including, but not limited to polymeric micelles, liposomes, dendrimers and gold/iron oxide NPs [27,29–31]. The immunomodulatory compounds can be either loaded inside the core or attached on the surface of the NPs. Through synthetic chemistry and NP engineering strategies, improved targeting effects and enhanced immune responses could be achieved by controlling the physicochemical properties of the NPs including particle size, particle shape, surface charge, surface chemistry and hydrophobicity, rigidity and targeting ligands (Fig. 1). For instance, controlling the NP size is an attractive strategy to achieve effective LN targeting and changing the particle shape significantly affect the interactions between NPs and macrophages, which both markedly influence the toxicity and immune responses induced by NPs [20,32–35]. Understanding the relationship between the various NP physicochemical properties and their lymphatic targeting abilities, in terms of tissue, cell, and sub-cellular targeting, is important to NP design as the carrier for vaccines and immunotherapy agents. In this review, we will discuss various approaches used to control the physicochemical properties of NPs, and elaborate on how these properties of immunomodulatory agent-loaded NPs influence lymphoid tissues and immune cells targeting.

2. Effect of NP size on lymphatic targeting

Particle size is one of the most important parameters that influences NP biodistribution and interactions with immune cells after administration. For polymeric and lipid NPs, particle size can be controlled by changing the physicochemical properties of the NP forming materials or by using various NP preparation methods such as flash nanoprecipitation, microfluidic devices, layer-by-layer self-assembly and particle replication in nonwetting templates (PRINT) technology, as previously reviewed [37]. More recently, our group has developed a new method termed Flash Nanocomplexation (FNC) for DNA or protein therapeutic-loaded NP preparation with good size control in a scalable and reproducible manner [38–43]. In addition, particle size of gold NPs can be easily controlled by tuning the preparation conditions [44]. These methods provide appealing platforms to investigate the size

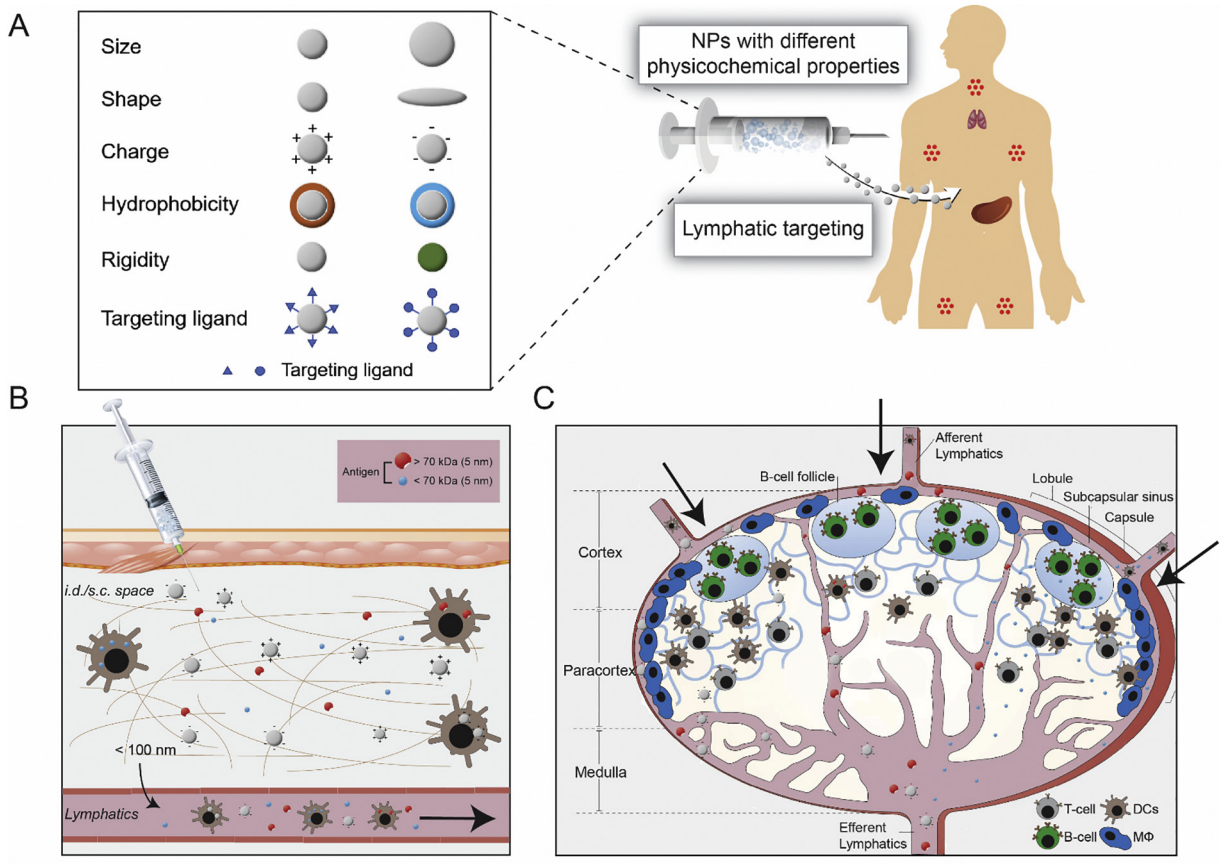

Fig. 1. (A) Schematic illustration of various NP physicochemical properties including size, shape, charge, hydrophobicity, rigidity and targeting ligand influence lymphatic targeting. (B) NPs and antigen below 100 nm in hydrodynamic diameter in the intradermal or subcutaneous space drain to the lymphatics. (C) The LN sieves NP and antigen in a size-dependent fashion, dictating which immune cell subsets process self or non-self-antigen cues. Modified from [36].

effect of NPs. In this section, the effect of particle size on LN targeting, biodistribution, interactions with immune cells, and immune response to the delivered antigens of NPs will be discussed.

2.1. Effect of NP size on LN targeting

Draining LNs have a high density of immature APCs, making them an attractive target for vaccines and therapeutics [45]. NP size has been shown as a key determinant for LN targeting and retention. Reddy *et al.* showed that small polypropylene sulfide (PPS) NPs stabilized by polyethylene glycol (PEG) or Pluronic (<50 nm) were more readily transported to dLNs and processed by immature dendritic cells (DCs) than large NPs (100 nm) by convective lymphatic drainage following intradermal (*i.d.*) administration [20,32]. The lower size limit for preferential lymphatic drainage targeting was found to be 8 nm by using dendritic polymers [46]. NPs below this size preferentially drain into the blood *via* absorption into capillary beds by passing through endothelial cell junctions. NPs above 8 nm travel primarily by convection and traverse the thick, negatively-charged extracellular matrix in a size- and charge-dependent manner [47,48]. These NPs can then cross the junctions between lymphatic endothelial cells (LECs) that line the lymphatic collecting system, and enter the collecting vessel's lumen (Fig. 2) [13]. This entry is facilitated by stress-induced stretching of anchoring filaments that adhere LECs to the extracellular matrix. The temporal stretching allows passage of soluble macromolecules *via* convection into the initial lymphatics [13]. This stretching is induced under peristaltic pressure driven by unidirectional fluid flow originating from Starling Forces that govern the passive exchange of water between the capillary bed and surrounding tissue [49].

Size discrimination originates from the interstitial extracellular matrix, which forms water pores that are about ~100 nm in diameter, and acts as a molecular sieve for convective transport [51]. NPs above 100 nm are retained at the injection site until uptake by epidermal or dermal DCs that then activate and upregulate chemokine receptor CCR7, and travel to the dLN through the lymphatics [52]. One strategy to avoid this size limitation in NP transport is by using *intra*-LN injection [53]. The size requirements for LN targeting differ from ideal size characteristics for targeting major APC populations in the LNs. Particulate and soluble matter in lymphatic fluid entering the LN through afferent lymphatic vessels are sorted by hydrodynamic size in the subcapsular

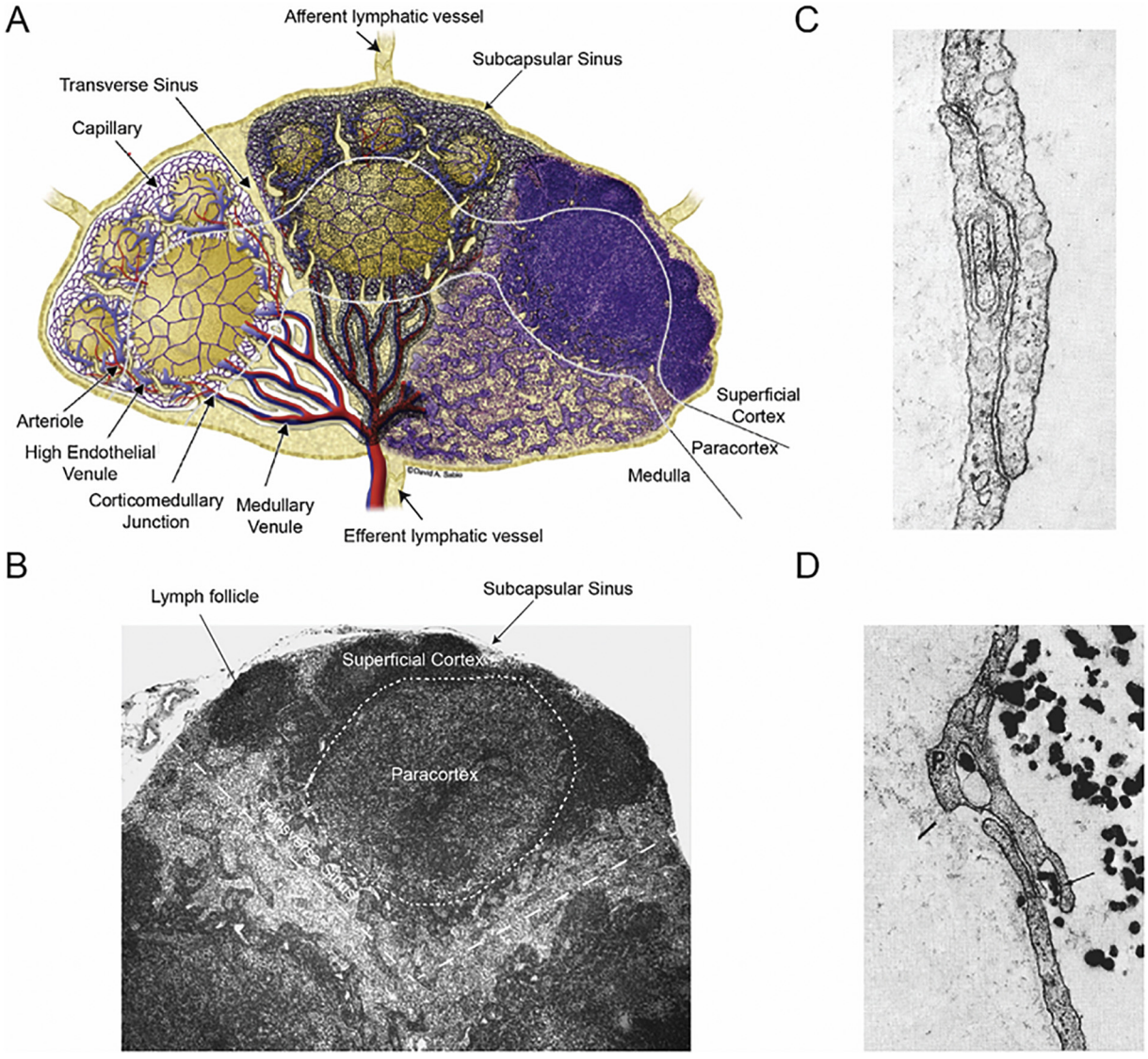

Fig. 2. LN anatomy. (A) LNs are composed of one or many functional units called lobules. Each lobule has the same features of superficial cortex, paracortex, and medulla regions. Antigen entering the LN by afferent vessels are filtered into the cortex region if <70 kDa, otherwise passing through the transverse sinuses and exiting the LNs by efferent vessel. (B) H&E micrograph of a LN highlighting critical features. (C) LEC junction with anchoring filaments. (D) Labeled particulates <100 nm can pass through the LEC junction. (A) and (B) reproduced with permission from [50]. (C) and (D) reproduced with permission from [11].

sinus. Macromolecules below 70 kDa (corresponding to a hydrodynamic radius of 4 nm) can traverse the CD169+ subcapsular macrophage lining by way of the reticular network, which penetrates into the paracortical zone containing the highest density of T lymphocytes and DCs [54,55]. Larger NPs are relegated to the subcapsular sinus region as they drain out the LN *via* the efferent lymphatic vessel, and are not taken up by any immune cells unless coated by complement; they are eventually released into the blood circulation *via* the thoracic duct or cisterna chyli [56].

2.2. Effect of NP size on biodistribution under disease conditions

Most NP trafficking studies use healthy mouse models to define the biodistribution of NPs after administration. However, within the context of different diseases, the distribution of NPs to the lymphatic system may greatly differ. Chen *et al.* investigated the effects of systemic inflammation on the distribution of spherical, fluorescently labeled polystyrene (PS) (20, 100, 500 nm) NPs after intravenous (*i.v.*) injection [57]. In non-inflamed conditions, the biodistribution of these NPs were as expected, with majority of the NP dose accumulating in the liver, lungs and spleen. However, after the introduction of lipopolysaccharide (LPS) and induction of systemic inflammation over a 16-hour period, there was a decrease in accumulated dose in the liver and lung, while there was an increase in NP retention in the spleen across all NP sizes. Using Evans Blue assay, they revealed that spleen had a much higher degree of blood vessel leakage than the other organs after treated with LPS. This might be the reason causing the increased retention of 20 nm NPs in the spleen at LPS-induced inflammatory condition. On the other hand, the increased retention of larger NPs in the spleen might associate with the higher uptake of these NPs by spleen leukocytes during inflammation. The magnitude of statistically significant differences between NP retention in control and LPS-induced systemic inflammation mice was directly associated with size, where 500 nm NPs saw the greatest increase in retention in the spleen, and 20 nm NPs had very little difference in biodistribution before and after systemic inflammation. A similar change in biodistribution occurs in the presence of a tumor, altering immune cell interactions with NPs by upregulating M2 macrophage polarization systemically and in secondary lymphoid organs, resulting in faster NP clearance relative to healthy mice [58]. This size- and organ-specific change in retention highlights the importance of pathology-specific systemic conditions in designing NP treatments.

2.3. Effect of NP size on immune responses

The immune response of NPs has been shown to be significantly affected by NP size. Kang *et al.* synthesized OVA-conjugated gold NPs (OVA-Au-NPs) with hydrodynamic diameters of 10, 22 and 33 nm and found that the 33 nm NPs had the best DC uptake *in vitro* and in the dLNs, while the 22 nm NPs had significantly higher polyfunctional CD8+ T cells [59]. In an EG7-OVA prophylactic lymphoma tumor model, the 22 nm NPs significantly prevented tumor growth compared to the 10 nm NPs, which had no significant difference compared to free OVA. Stano *et al.* used an OVA-conjugated Pluronic stabilized PPS NP to compare the extremes of sizes, 30 and 200 nm, to determine which NP size best elicits a cellular and humoral response after intranasal administration [60]. The 200-nm PPS NPs increased OVA-specific OT-I CD8+ T cell and OT-II CD4+ T cell proliferation *ex vivo* in a dose-depended manner compared to 30-nm PPS NPs. *In vivo*, the 200-nm PPS NPs induced a statistically higher fraction of polyfunctional lung CD4+ T cells (secreting INF-γ, TNF-α and IL-2) compared to the 30-nm PPS NPs, while there was no significant difference in elicited polyfunctional lung CD8+ T cells. Similarly, Zhou *et al.* engineered Toll-like receptor-9 (TLR-9) agonist CpG oligodinucleotide (ODN)-conjugated Au-NPs with finer gradations of change in NP diameter (15, 30, 40, 60, 80 nm), and found that the 80 nm NPs had the greatest antigenic presentation and stimulatory capacity in bone marrow-derived dendritic cells (BMDCs) as measured by H-2Kb (SIINFEKL) and CD40 flow cytometric surface staining, respectively [61]. This work highlights how controlling NP size to control antigenic presentation can be used to enhance cell-based immunotherapeutics already used in the clinic.

As suggested above, the impact of various immunostimulatory adjuvants can be dictated by NP size and packaging. It was thought that CpG-ODN stimulatory activity was dictated by sequence motifs and their secondary and tertiary structures alone, thus explaining why different classes of CpG (CpG-A, CpG-B, CpG-C) elicit differential plasmacytoid DC (pDC) activation and maturation, IL-1β secretion and IFN-α production [62]. It was later determined that these molecules' stimulatory capabilities and responses were not caused by their sequence motifs or relative unmethylated CG content, but rather that the mechanism was linked to CpG compartmentalization into early or late endosomes [62]. IL-1β secretion correlated with sequestration of CpGs in early endosomes, while pDC maturation was linked to CpG localization in LAMP-1-rich late endosomes, regardless of CpG sequence. Controlling this localization by aggregating or breaking up CpG aggregates with different sequences and class (CpG-A, CpG-B, CpG-C) thus allows for control of CpG activity. Taking advantage of this insight, multiple groups have conjugated CpGs directly to the NP surface and controlled NP size to modulate immunostimulation and downstream immune response [63–65]. Conjugating CpG2006–a CpG-B that preferentially induces pDC activation and elicits little IFN-α secretion when delivered in free form–onto 3–4 nm sized silicon NPs skewed CpG-B activity away from pDC activation and towards IFN-α secretion [63]. Along with particle size, surface density of adjuvants on NP surface may also affect the immune response. Controlling the CpG surface density on poly(lactic-*co*-glycolic acid) (PLGA) NPs (~100 nm) and PLGA microparticles (2 μm) skewed results towards a Th1 *vs.* Th2 immune response, with the NPs eliciting more of a Th2 response unless NPs had a high CpG density, where the response was skewed towards Th1. The 2 μm microparticles always led to a Th1-biased response regardless of CpG surface density (Fig. 3) [64]. Smaller gold NPs of 13 nm (sphere), 40 nm (star) and 50 nm (sphere) with the same CpG surface density also had differential responses, where 40 nm and 50 nm NPs had greater uptake, NF-κB activation and cytokine secretion in murine macrophages RAW-BLUE reporter cells relative to 13 nm NPs [65]. Similar control of aluminum salt adjuvant activity by controlling NP size has been demonstrated. Historically, alum salts yield only Th2 antibody responses, which are hallmarked by weak cellular immune response and poor immune memory induction. Typically, alum salts are mixed directly with antigens prior to injection, creating 2–20 μm sized alum/antigen depots at the injection site. Controlling this alum/antigen depot size by generating well-controlled NP and microparticle structures allowed for control of adjuvant immunogenicity, activation and injection site inflammation [66,67]. Li *et al.* synthesized aluminum hydroxide NPs (200 nm) or microparticles (9.3 μm) surface-coated with OVA to investigate size-dependent immune response [67]. Compared to the microparticles, the NPs had a greater reduction in inflammation at the site of injection and an increase in antibody titer in a mouse model. In addition, only the NPs prevented tumor growth in a B16-OVA tumor model [67]. These results suggest that immune cells sense not only the pathogen-associated molecular patterns, but also their spatial presentation and together, they influence the appropriate immune response (*e.g.* Th1 for small viruses, Th2 for bacteria). The NP systems discussed in this section are summarized in Table 1.

3. Effect of NP shape on lymphatic targeting

The continuous development of NP preparation techniques such as PRINT, step and flash imprint lithograph (S-FIL) and membrane stretching to control particle shape, has further enabled research efforts to investigate the shape effect of NPs [69,70]. In this section, we will discuss the effects of particle shape on the interactions with macrophages

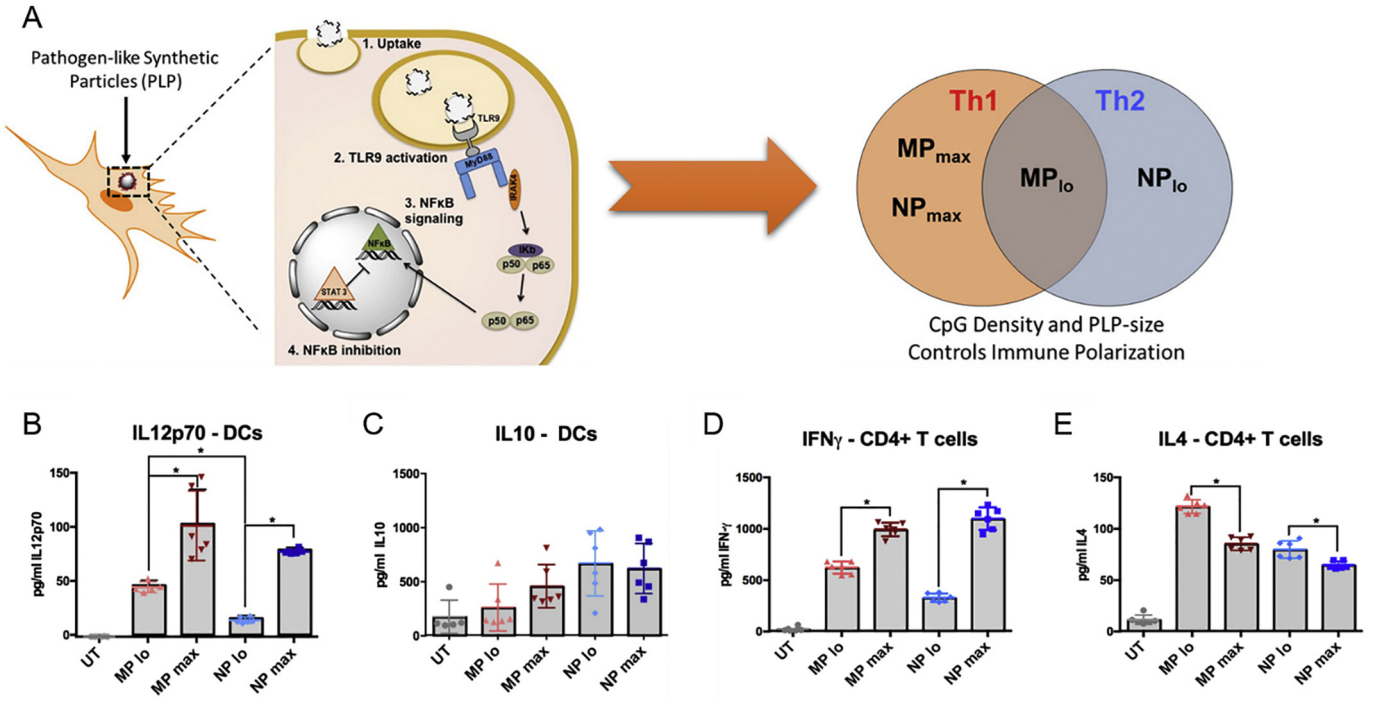

Fig. 3. NP size and CpG surface density influences DC and T cell cytokine profiles. (A) Schematic illustration depicting the mechanism of action of PLPs and how CpG density and PLP-size impacts the biological response with regards to the systemic immune polarization observed after treatment of each formulation. Maximum density NPs promoted greater secretion of IL12p70 inactivated BMDCs 24 h after initial treatment. (C) IL-10 production was low regardless of treatment 24 h after initial treatment. (D) IFN-γ secretion of CD4+ transgenic T-cells (OT-II) that were co-cultured with activated BMDCs mirrored IL12p70 profiles, with the maximum density NP-treated DCs inducing greater IFN-γ production. (E) IL4 secretion patterns in OT-II CD4+ T-cells demonstrate an inverse pattern relative to (C), with low-density formulation inducing a greater secretion of IL-4 than their maximum density NP counterparts. Reproduce with permission from [64].

and DCs, and the immune response, as well as the application of NPs of various shapes for immunotherapy.

3.1. Effect of NP shape on cellular uptake by macrophages and DCs

Regardless of the administration route, NPs introduced into the body may be recognized and internalized by macrophages through phagocytosis. For those NPs that are not for macrophage targeting, this process may significantly affect the delivery efficiency to the desired cell populations. NP shape has long been known to influence the phagocytic efficacy of macrophages. For instance, worm-like filomicelles delivering the anti-cancer drug paclitaxel showed 10 times longer blood circulation time than their spherical counterparts in both mice and rats [71]. It was speculated that the macrophages had more difficulty phagocytosing the filomicelles compared to the spherical micelles in both cell culture and flow conditions [71]. Similarly, Samir and his co-workers also found that worm-like particles with aspect ratio >20 were negligibly phagocytosed compared to spherical particles with the same volume [72]. The contact angle of the particle with macrophage was important in controlling the phagocytosis efficiency of such particles [73]. When the contact angle was small, the macrophage membrane formed an actin cup and ring structure to achieve successful internalization of the particles, while with a large contact angle, the energy required to form the actin cup to cover the particles was too high to induce phagocytosis [73]. Thus, the worm-like particles could only be internalized when they contacted with the macrophages along their long axis, which explained why worm-like particles were phagocytosed less efficiently than the spherical particles by macrophages [73]. By taking advantage of this, Wibroe *et al.* changed the particle geometry from spherical shape to either rod- or disk-shape to delay the recognition by pulmonary macrophages within the first few minutes after *i.v.* injection, which effectively mitigated the cardiopulmonary reactions after NP injection in pigs [74]. The shape effect on phagocytosis is also associated with size. Spherical NPs with sizes of 0.5-, 1- and 3.6-μm, were stretched to form oblate ellipsoids and prolate ellipsoids to investigate the shape and size effects on phagocytosis [75].For small particles derived from 0.5 and 1 μm particles, the phagocytes were more efficient at engulfing oblate ellipsoids, followed by spheres, and then prolate ellipsoids. However, no differences in phagocytosis were observed for the large particles (derived from 3.6-μm particles) [75].

NP shape also affects the interactions of NPs with DCs. It was found that disc-shape NPs could be internalized in a much higher degree than rod-shape NPs with similar volume and similar largest surface area by BMDCs [76]. In another study, nanofibers showed enhanced uptake than spherical NPs in DCs (CD11c+) and plasmacytoid DCs (CD11c+/B220+) isolated from splenocytes [77].

3.2. Effect of NP shape on immune responses

The shape effect of NPs on immune responses has also been investigated in both *in vitro* and *in vivo*. For the rod-shaped aluminum oxide NPs with long and short aspect ratios of 6.2 and 2.1, only the long-type NPs showed the ability to increase the population of neutrophils and monocytes, and were more effective in inducing the co-expression of CD80 and CD86 on splenocytes, decreasing the expression of CD195 compared with the short-type NPs upon *i.v.* injection [68]. Although the spherical NPs had higher cell uptake than the cylindrical NPs, the long cylindrical NPs was far more effective in inducing the secretion of IL-6 than spherical NPs and short cylindrical NPs in murine macrophages RAW 264.7 cells [78]. When NPs with different shapes were used as adjuvants for antigen delivery, they significantly influenced the immune responses elicited by the loaded antigens. For instance, Samir and his co-workers prepared a set of PS NPs (two spherical NPs with diameters of 193 and 521 nm, and two rod-shape NPs derived from the spherical NPs with 376 nm and 1530 nm in length) and decorated OVA on the surface to investigate the size- and shape-depended immune response [79]. Results showed that immune responses shifted from a Th1-biased response to a Th2-biased response

Table 1
Examples of NPs used to investigate the effect of size on lymphatic targeting.

NP forming materials	Payload/dye	Main characteri-zations	Immune cells	Animal model	R.A.	Key findings	Ref.
PEG-stabilized PPS	Fluorescein or Alexa Fluor 488	Size: 20, 45 and 100 nm		BALB/c mice	*i.d.*	Small size NPs (20 and 45 nm) had better LN targeting and higher level of DC uptake in the LN than the large NPs (100 nm).	[20]
Pluronic stabilized PPS	OVA	Size: 25 and 100 nm; Surface groups: OH *vs.* OCH_3		BALB/c, C57BL6 and C3−/−, OT-II Tg and CD45.1 mice	*i.d.*	Small size NPs had better LN targeting and higher level of DC uptake in the LN than the large NPs; Combination of small size and *in situ* complement activation elicited strong immune responses.	[32]
PLGA-*b*-PEG	Cy7.5 and Alexa Fluor 488	Size: 20, 40, and 100 nm		SKH1-Elite and CD1 mice	*s.c.*	Size-dependent gradient in lymphatic targeting kinetics, fraction of injected dose in LN, NP uptake by DCs, paracortex penetration, and retention in draining LN, all following the trend of 20 > > 40 > 100 nm. Suggests that NPs smaller than 30 nm exhibit optimal drainage kinetics and LN retention.	[35]
PS	Molecular Probes® FluoSpheres® proprietary yellow-green dye	Size: 20, 100 and 500 nm		FVB mice at inflammatory condition induced by LPS	*i.v.*	Under inflammatory condition, accumulation of NPs increased in the spleen; the 500-nm NPs showed the most significant difference compared with that at healthy condition.	[57]
Gold	OVA	Size: 10, 22 and 33 nm	DC2.4 and OT-1 T cells	EG7-OVA tumor model	*s.c.*	The 33-nm NPs had the best DC uptake *in vitro* and in the dLNs, while the 22-nm NPs had significantly higher polyfunctional CD8 + T cells; The 22-nm ONPs significantly prevented tumor growth compared to the 10-nm NPs.	[59]
Pluronic stabilized PPS	OVA	Size: 30 and 200 nm		C57BL/6, OT-II and OT-I OVA transgenic mice	*i.n.*	The 200-nm NPs induced a statistically higher fraction of polyfunctional lung CD4+ T cells compared to the 30-nm NPs *in vivo*.	[60]
Gold	CpG; OVA	Size: 15, 30, 40, 60 and 80 nm	BMDCs			The 80-nm NPs had the greatest antigenic presentation and stimulatory capacity.	[68]
Silicon	CpG-B	Size: 3–4 nm	PBMCs			Conjugating CpG-B onto silicon NPs skewed CpG-B activity away from pDC activation and towards IFN-α secretion.	[63]
PLGA	CpG	Size: 100 nm and 2000 nm CpG density: low and high	BMDCs			The 100-nm NPs elicited more of a Th2 response unless NPs had a high CpG density, where the response was skewed towards Th1; The 2000-nm NPs led to a Th1-biased response regardless of CpG surface density.	[64]
Gold	CpG	Size: 13 nm spheres, 50 nm spheres, and 40 nm stars	RAW-BLUE			The 40- and 50-nm NPs had greater uptake, NF-κB activation and cytokine secretion in RAW-BLUE cells relative to 13-nm NPs.	[65]
Alum	OVA and *Bacillus anthracis* protective antigen protein	Size: 112 nm and 9.3 μm	BMDCs, DC2.4 and J774A.1 cells	B16-OVA tumor model	*s.c.*	The NPs had a greater reduction in inflammation at the site of injection and an increase in antibody titer in a mouse than the 9.3-μm macroparticles; Only the NPs prevented tumor growth in a B16-OVA tumor model.	[67]

PPS: polypropylene sulfide; PS: polystyrene; PLGA: poly(lactic-*co*-glycolic acid); Alum: aluminum; OVA: ovalbumin; BMDCs: bone marrow-derived dendritic cells; PBMCs: Peripheral blood mononuclear cells; LPS: Lipopolysaccharide; R.A.: route of administration; *i.d.*: intradermal; *i.v.*: intravenous; *i.n.*: intranasal; *s.c.*: subcutaneous; Ref.: Reference.

when the maximum particle length of the NPs increased (Fig. 4) [79]. Among all the NPs, the small spherical NPs elicited the strongest both Th1-biased and Th2-biased responses [79]. In another case, Niikura *et al.* engineered four cetyltrimethylammonium bromide (CTAB)-coated gold NPs including spheres (20 and 40 nm in diameter), rod (40 × 10 nm) and cubic (40 × 40 × 40 nm) for the West Nile virus envelope (WNVE) protein delivery [80]. Compared to other NPs, 40 nm spherical NPs elicited the highest level of WNVE antibody level in C3H/HeNJc1 mice after intraperitoneal (*i.p*) injection. In APC cells (BMDCs and RAW264.7), rod NPs showed the highest cellular internalizations and induced the highest level of IL-1β and IL-18 secretions, while 40 nm spherical NPs and cube NPs induced higher levels of the secretion of the pro-inflammatory cytokines including TNF-α, IL-6, IL-12 and GM-CSF than other NPs [80]. The NP systems discussed in this section are summarized in Table 2.

4. Effect of NP surface charge on lymphatic targeting

Surface charge is an important NP feature that influences the NP stability and the interactions of NPs with biological systems, which can be controlled by tuning the ratio of cationic and anionic NP forming materials or coating the surface of NPs with materials with different charges. In this section, how the surface charge affects the cellular uptake by APCs, immune response, LN targeting ability and biodistribution of NPs will be discussed.

4.1. NP uptake by APCs is dependent on both NP surface charge and size

Due to the negative surface charge of the cell membrane, cationic NPs typically exhibit higher cell internalization compared to anionic and natural NPs. One study showed that Chitosan-based NPs of the same particle size but different zeta potentials (+39.25, +0.51 and −45.84 mV, named P-NPs, M-NPs and N-NPs respectively) presented differentiated cellular uptake with the P-NPs showing higher cellular uptake than the other two NPs in eight different cell lines including carcinoma, epithelial, endothelial, fibroblast and megakaryoblastic cells [84]. However, predicting the cellular uptake as a function of the charge of a NP in macrophages and DCs is more complicated. In BMDCs, 100 nm cationic NPs had higher cellular uptake than 100 nm anionic NPs, while 200 nm anionic NPs showed higher cellular uptake than 200 nm cationic NPs [85]. Surface charge had negligible effect on cellular uptake for 500 nm NPs [85]. Thus, the results indicated that the charge effect of NPs on cellular uptake in macrophages and DCs were also dependent on the particle size.

4.2. Effect of NP surface charge on biodistribution and immune responses

Surface charge also significantly influences biodistribution, and thus immune response to NPs. In a recent study published by Kranz and Diken *et al.*, it was found that changing the surface charge of mRNA-

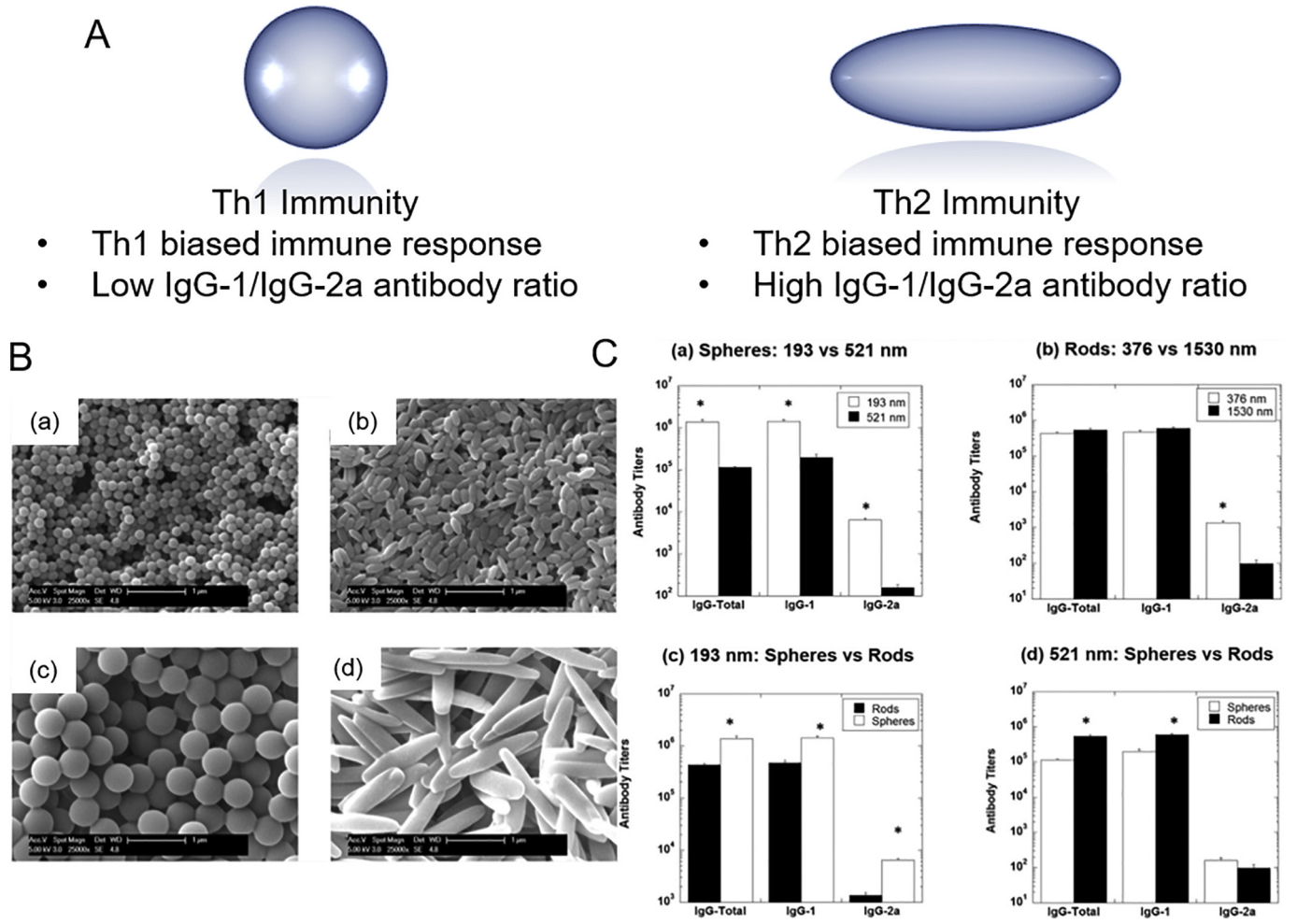

Fig. 4. Size and shape-dependent modulation of immune response: (A) Immune response as function of the size and shape of NPs. (B) SEM images of particles with different sizes and shapes. SEM image of OVA conjugated ps particles for: (a) OVA-Spheres-193, (b) OVA-Rods-376, (c) OVA-Spheres-521 and (d) OVA-Rods-1530. Scale bars = 1 μm. (C) Shape, size and volume effect on antibody titer production. The antibody titers obtained at 3rd week after booster immunization were used to estimate the effect of varying size (a and b) and equivolume shape (c and d) on antibody (IgG-total, IgG-1 and IgG-2a) generation. * indicates that the values are significantly higher compared to other groups, respectively ($p < 0.001$). Each data point represents mean ± STDEV ($n = 4$). Reproduced with permission from [79].

lipoplexes (RNA-LPX) from positive to negative through enhancing the charge ratio of mRNA to cationic lipids (*e.g.* DOTMA and DOPE) shifted the distribution of RNA-LPX from the lungs to the spleen after *i.v.* injection (Fig. 5A–C) [86]. In addition, negatively charged RNA-LPX had high accumulation and gene expression in DCs and macrophages within various lymphoid compartments including spleen, LNs and bone marrow. Administration of the negatively-charged antigen-encoded RNA-LPX triggered interferon-α (IFNα) release, and induced strong effector and memory T-cell responses as well as mediated rejection of progressive tumors (Fig. 5D) [86]. In an ongoing phase I clinical trial, the first three melanoma patients treated with a low-dose RNA-PLX encoding shared tumor antigens showed strong INF-α expression and antigen-specific T-cell responses (Fig. 5E) [86]. Huang's group has also showed that for NPs of same size, negatively-charged lipid/calcium/phosphate (LCP) NPs (zeta potential: −19.9 ± 4.1 mV) had greater LN accumulation than the positively-charged LCP NPs (zeta potential: +21.3 ± 2.1 mV) after *i.v.* injection [87]. However, positively charged LCP NPs exhibited higher gene expression level compared to negatively charged LCP NPs in LNs, which can be attributed to the higher cellular uptake and greater endosome escaping ability of the positively charged NPs [87].

Doddapaneni *et al.* prepared three types of NPs including neutral, partially-negatively charged and fully-negatively charged NPs with zeta potentials of −6.4 ± 0.24, −19.2 ± 2.15 and −37.6 ± 1.02 mV, respectively, to investigate the charge effect on LN trafficking patterns. The results showed that the neutral NPs and partially-charged NPs were effective in lowering the number of melanocytes at proximal LNs and both proximal and distal LNs respectively, while the fully-charged NPs had no effect on either LNs [83]. Fromen *et al.* investigated the impact of the NP charge in the immune response using two OVA conjugated rod NPs with positive or negative surface charge upon pulmonary administration [33]. Results showed that the OVA-conjugated cationic NPs induced high systemic and lung antibody titers and increased the population of germinal center B-cells and activated CD4+ T-cells in lung dLNs, while OVA-conjugated anionic NPs had no effect [33]. In a subsequent study, they found that both cationic and anionic NPs were capable of trafficking to the dLNs after pulmonary administration [81]. Cationic NPs showed lower cell internalization in lung alveolar macrophages but higher cell association with lung CD11b+ and CD103 + DCs when compared with anionic NPs [81]. As a result, the cationic NPs induced upregulation of CCL2 and CXC10 in the lung [81]. In a more recent study, it was fond that cationic NPs and anionic NPs had similar effects in stimulating the release of IL-1β from BMDCs, however, the release of IFN-γ from T cells after incubation with BMDCs treated with various NPs was greatest for cationic NPs, followed by neutral NPs and lastly anionic NPs [82].

Myeloid-derived suppressor cells (MDSCs) are one of the major populations of immune cells at the tumor microenvironment and

Table 2
Examples of NPs used to investigate the effect of shape on lymphatic targeting.

NP forming materials	Payload/dye	Main characteri-zations	Immune cells	Animal model	R.A.	Key findings	Ref.
PEG-PEE and PEG-PCL	Paclitaxel/PKH26	Shape: spheres and worms		C57 mice and Sprague–Dawley rats	*i.v.*	Worm-like NPs showed 10 times longer blood circulation time than their spherical counterparts in both mice and rats.	[33]
PS	Coumarin	Shape: spheres and worms	Rat macrophage cells NR8383			Worm-like particles with aspect ratio >20 were negligibly phagocytosed compared to spherical particles with the same volume.	[81]
PS		Shape: spheres, Oblate ellipsoids, Prolate ellipsoids, Elliptical disks, Rectangular disks and UFOs	NR8383 and J774			Small contact angle of the particle with macrophage induced fast phagocytosis.	[82]
PS		Shape: spheres, rods and discs		Pig	*i.v.*	Changing the particle geometry from spherical shape to either rod- or disk-shape delayed the recognition by pulmonary macrophages within the first few minutes.	[34]
PS		Shape: spheres, oblate ellipsoids and prolate ellipsoids Size: 0.5, 1 and 3.6 μm	RAW264.7			For small particles, the phagocytes were more efficient at engulfing oblate ellipsoids, followed by spheres, and then prolate ellipsoids.; No differences in phagocytosis were observed for the large particles with different shapes.	[83]
PEGDA	Fluorescein	Shape: rods and discs	BMDCs			Disc-shape NPs could be internalized in a much higher degree than rod-shape NPs with similar volume and similar largest surface area.	[76]
Peptide self-assembled NPs	CpG	Shape: spheres and rods	DCs and plasmacytoid DCs isolated from splenocytes			Rod-shape NPs showed enhanced uptake than spherical NPs in DCs and plasmacytoid DCs.	[77]
Aluminum oxide		Shape: rods with aspect ratios of 6.2 and 2.1		ICR mice	*i.v.*	Only the long-type NPs showed the ability to increase the population of neutrophils and monocytes, and were more effective in inducing the co-expression of CD80 and CD86 on splenocytes, decreasing the expression of CD195 compared with the short-type NPs.	[68]
PDLLA-b-PAA and PLLA-b-PAA	Fluorescein	Shape: spheres and rods	RAW 264.7			The spherical NPs had higher cell uptake than the rod NPs; The long rod NPs was far more effective in inducing the secretion of IL-6 than spherical NPs and short rod NPs.	[62]
PS	OVA	Shape: two spherical NPs with diameters of 193 and 521 nm and two rod-shape NPs derived from the spherical NPs with 376 nm and 1530 nm in length	DC2.4	BALB/c mice	*s.c.*	The immune responses shifted from a Th1-biased response to a Th2-biased response when the maximum particle length of the NPs increased; The small spherical NPs elicited the strongest both Th1-biased and Th2-biased responses than other NPs.	[63]
Gold	WNVE	Shape: spheres (20 and 40 nm), rods and cubes	BMDCs and RAW264.7	C3H/HeNJc1 mice	*i.p.*	The 40 nm spherical NPs elicited the highest level of WNVE antibody level than other NPs; The rod NPs showed the highest cellular internalizations and induced the highest level of IL-1β and IL-18 secretions in APC cells; The 40 nm spherical NPs and cube NPs induced higher levels of the secretion of the pro-inflammatory cytokines including TNF-α, IL-6, IL-12 and GM-CSF than other NPs in APC cells.	[64]

PEG-PEE: polyethylene glycol-polyethyl ethylene; PEG-PCL: polyethylene glycol-polycaprolactone; PS: polystyrene; PEGDA: polyethylene glycol diacrylate; PDLLA-b-PAA: poly(D,L-lactide)-b-poly-(acrylic acid); PLLA-b-PAA: poly(Llactide)-b-poly(acrylic acid); OVA: ovalbumin; WNVE: West Nile virus envelope; BMDCs: bone marrow-derived dendritic cells; R.A.: route of administration; i.v.: intravenous; s.c.: subcutaneous; i.p.: intraperitoneal; Ref: reference.

have potent immune suppressive activity [90]. It has been shown that cationic polymers (*e.g.* cationic dextran and polyethyleneimine (PEI)) have the potential to re-polarize MDSCs at tumor site from M2 immunosuppressive phenotype to M1 anti-tumor phenotype [91]. By taking advantage of this, Wu *et al.* prepared PEI coated magnetic cationic NPs to combine with radiotherapy for brain tumor treatment. Due to the cytotoxicity to the tumor cells under radiation and the re-polarization effect on MDSCs, these NPs significantly prolonged the survival time of both immunocompetent and athymic mice with glioma [34]. Neutrophils are the most abundant leukocytes in the blood and the "first responders" against foreign materials that enter our bodies [92]. It was found that changing the surface charges of both polymeric and lipid NPs from negative to positive by adding cationic surfactants caused cytotoxicity and inflammatory response to human neutrophils [93].

It is important to point out that the surface properties of NPs is significantly changed once in contact with physiological conditions, due to the formation of protein corona [94,95]. In a study where superparamagnetic iron oxide NPs (SPIONs) with different surface charges were incubated in serum, cationic and neutral NPs preferentially led to serum protein adsorption compared to anionic NPs [96]. The NP systems discussed in this section are summarized in Table 3.

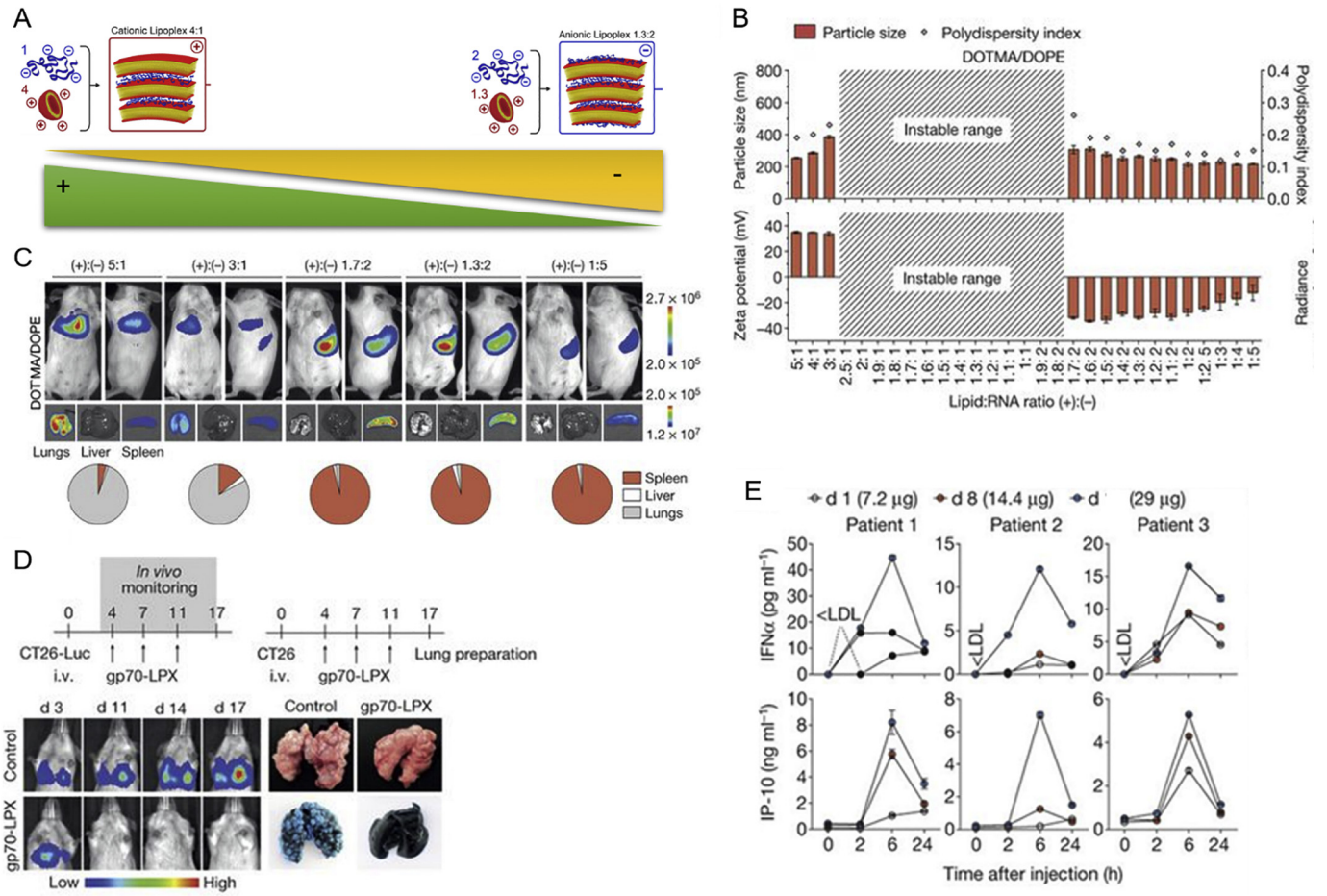

Fig. 5. mRNA-lipoplexes quality attributes and impact in biodistribution and treatment of melanoma patients. (A) Impact of mRNA and lipid composition on charge and structure of lipoplexes. (B) Particle size, polydispersity index (top) and zeta potential (bottom) (n = 3) of RNA-lipoplexes constituted with DOTMA/DOPE liposomes and Luc-RNA at various charge ratios. (C) Bioluminescence imaging of BALB/c mice (n = 3) after *i.v.* injection of Luc-lipoplexes at various charge ratios. Pie charts show relative contribution of each organ to total signal. (D) CT26-Luc growth and CT26 tumor load in lungs of BALB/c mice (n = 4–7) immunized *i.v.* with gp70-lipoplexes. (E) Serum cytokines before (0 h) and after injection of intra-patiently escalated doses of RNA-lipoplexes vaccines encoding four tumor antigens (NY-ESO-1, MAGE-A3, tyrosinase and TPTE). (A) Reproduced with permission from [88,89]; (B-E) Reproduced with permission from [86].

5. Effect of NP surface hydrophobicity on lymphatic targeting

Several strategies have been commonly used to control the hydrophobicity of NPs, such as (a) forming NPs using amphiphilic polymers with different hydrophobic segments [97]; (b) grafting side chains of varying degrees of hydrophobicity onto the main NP chain, forming polymers [98–101]; (c) modifying the surface of NPs with various functional groups [82,102,103]; and (d) preparing NPs by blending two polymers with different degrees of hydrophobicity [104]. In addition, to further investigate the effects of hydrophobicity, NPs fabricated using polymers with similar structures but different hydrophobicity have also been adopted [105–107]. In this section, we will discuss how hydrophobicity affects the antigen-loading ability and release profile, LN targeting and retention effects, DC uptake and activation and immune response.

5.1. Effect of NP hydrophobicity on antigen release and integrity

Hydrophobicity of the NP-forming materials can significantly influence the antigen release profile and functional preservation, and subsequently influence the immune response. For instance, Petersen *et al.* designed and synthesized four polyanhydride polymers for the delivery of bacillus anthracis protective antigen (PA) with the purpose of selecting the best nanoparticulate formulation to preserve the immunogenicity of PA during fabrication, storage and administration [97]. The four polymers were polymerized based upon three monomers, sebacic anhydride (SA), 1,6-bis(pcarboxyphenoxy) hexane (CPH) and 1,8-bis(p-carboxyphenoxy)-3,6-dioxaoctane (CPTEG), at different ratios. PA-loaded NPs prepared using these four polymers demonstrated sustained PA release over 2 months, with 20:80 CPTEG:CPH and 50:50 CPH:SA NPs showing slower PA release than 50:50 CPTEG:CPH and 20:80 CPH:SA NPs. Compared with the two CPH:SA polymers, the two amphiphilic polymers CPTEG:CPH were better at preserving the bioactivity and immunogenicity of PA during the fabrication process and in *in vivo* applications. Moreover, the amphiphilic polymer with a longer hydrophobic chain (20:80 CPTEG:CPH) preserved the biological activity of PA more effectively than the one with shorter hydrophobic chain (50:50 CPTEG:CPH) at 40 °C, 25 °C and 4 °C during a 4 month storage period.

5.2. Effect of NP hydrophobicity on LN drainage

The LN drainage and retention effect of NPs can also be influenced by the hydrophobicity. NPs with high hydrophobicity tend to form large aggregations at injection site, which decreases LN drainage. On the other hand, increasing the hydrophobicity can also enhance the interactions between NPs and immune cells, leading to increased cell-mediated NP uptake, LN trafficking and LN retention [108]. Thus, the hydrophobicity/hydrophilicity balance is an important factor that needs to be considered in designing LN-targeted NPs. In one particular

Table 3
Examples of NPs used to investigate the effect of surface charge on lymphatic targeting.

NP forming materials	Payload/dye	Main characteri-zations	Immune cells	Animal model	R.A.	Key findings	Ref.
Layer-by-layer NPs with PS beads core	Fluore-scein	Charge: positive (zeta potential: ~ +30 mV) and negative (zeta potential: ~−30 mV)	BMDCs			100 nm cationic NPs had higher cellular uptake than 100 nm anionic NPs; 200 nm anionic NPs showed higher cellular uptake than 200 nm cationic NPs; Surface charge had negligible effect on cellular uptake for 500 nm NPs.	[85]
Lipid	mRNA	Charge: negative		BALB/c mice, C57BL/6 mice, B16-OVA and CT26 tumor models	*i.v.*	Changing charge from positive to negative shifted the distribution of RNA-LPX from the lungs to the spleen; Negative charge NPs triggered interferon-α (IFNα) release, and induced strong effector and memory T-cell responses.	[86]
LCP		Charge: positive (zeta potential: +21.3 mV) and negative (zeta potential: −19.9 mV)		C57BL/6 mice and nude mice	*i.v.*	Negatively-charged NPs had greater LN accumulation than the positively-charged NPs; Positively charged NPs exhibited higher gene expression level compared to negatively charged NPs in LNs.	[87]
PEG-PCL	Docetaxel, evero-limus and LY294002	Charge: neutral (zeta potential: −6.4 mV), partially-negative (zeta potential: −19.2 mV) and fully-negative (−37.6 mV)		Metastatic melanoma mice models	*s.c.*	Neutral NPs and partially-charged NPs were effective in lowering the number of melanocytes at proximal LNs and both proximal and distal LNs respectively, while fully-charged NPs had no effect on either LNs.	[83]
PRINT NPs formed by TPO, AEMA, diacrylate PEG, mono-acrylate TEG	OVA	Charge: positive (zeta potential: +37 mV) and negative (zeta potential: −38 mV)		C57BL/6 mice	*p.a.*	Cationic NPs induced high systemic and lung antibody titers and increased the population of germinal center B-cells and activated CD4+ T-cells in lung dLNs, while anionic NPs had no effect; Cationic NPs showed lower cell internalization in lung alveolar macrophages but higher cell association with lung CD11b + and CD103+ DCs when compared with anionic NPs.	[33,81]
Silica NPs modified with PAA		Charge: zeta potential ranging from −42 mV to +38 mV	BMDCs and OT-I T cells			Cationic NPs and anionic NPs had similar effects in stimulating the release of IL-1β from BMDCs; The release of IFN-γ from T cells after incubation with BMDCs treated with various NPs was greatest for cationic NPs, followed by neutral NPs and lastly anionic NPs.	[82]
Magnetic NPs coated with PEI		Charge: positive (zeta potential: ~ +40 mV)	MDSCs isolation from bone marrow	CT2A glioma model	*i.c.*	Positively charged NPs repolarized MDSCs and prolonged the survival time of both immunocompetent and aythmic mice with glioma when combined with radiotherapy.	[34]
Lipid NPs and polymeric NPs		Charge: lipid NPs (−42.9, +52.0 and +51.5 mV); polymeric NPs (−5.6, +28.9 and +39.4 mV)	Human neutron-phils			Cationic NPs induced strong cytotoxicity and inflammatory responses to human neutrophils.	[93]
Superparamagnetic iron oxide NPs coated with PVA, SiO_2, TiO_2 or gold		Charge: zeta potential ranging from −48 mV to +37 mV				Cationic and neutral NPs preferentially led to serum protein adsorption compared to anionic NPs.	[96]

LCP: lipid/calcium/phosphate; PEG-PCL: polyethylene glycol-polycaprolactone; PRINT: particle replication in nonwetting templates; TPO: diphenyl(2,4,6-trimethylbenzoyl)phosphine oxide; AEMA: 2-aminoethyl methacrylate hydrochloride; TEG: tetra(ethylene glycol); PAA: poly(amino acid); PEI: polyethylene imine; PVA: polyvinyl alcohol; mRNA: messenger RNA; OVA: ovalbumin; BMDCs: bone marrow-derived dendritic cells; MDSCs: Myeloid-derived suppressor cells; R.A.: route of administration; *i.v.*: intravenous; *s.c.*: subcutaneous; *p.a.*: pulmonary administration; *i.c.*: intracranial; Ref.: reference.

study, Rao *et al.* found that the PP (PLGA-PMA:PLA-PEG) NPs with lower hydrophobicity showed higher LN accumulation than PS NPs with higher hydrophobicity upon subcutaneous (*s.c.*) injection in rats [107]. In another example, the more hydrophobic NPs generation-5 polypropylenimine dendrimer and Gadomer-17 showed higher axillary LN accumulation than the less hydrophobic poly(amidoamine) (PAMAM) dendrimer-based agents of similar sizes in mice after mammary gland injection for sentinel node imaging [46]. These studies thus highlight the role of hydrophobicity in controlling the LN targeting effect of NPs.

5.3. Effect of NP hydrophobicity on DC uptake and activation

Hydrophobicity can also influence the immune cell targeted by NPs. Akashi's group prepared NPs with different hydrophobicity using amphiphilic poly(g-glutamic acid)-*graft*-L-phenylalanine ethyl ester (PGA-*g*-Phe) with various grafting degrees of hydrophobic side chains for OVA delivery [98]. The results demonstrated that BMDC uptake and BMDC activation increased with increasing hydrophobicity of the NPs. Additionally, after *s.c.* injection of these NPs in mice, the cellular immune response increased when the grafting ratio was increased from 43% to 65%, but then decreased when the grafting ratio was increased from 65% to 71%, illustrating that a hydrophobic/hydrophilic balance needs to be achieved for effective cellular immune activation. In another study, Moyano *et al.* modified the 2 nm gold NPs with various surface functional groups to investigate the influence of surface hydrophobicity on cytokines expression levels both *in vitro* and *in vivo* (Fig. 6A) [102]. PEG was employed as a linker between gold core and surface functional groups to avoid the possible background effects caused by gold NPs (Fig. 6B). The results demonstrated that after injection of these NPs into mice, the levels of cytokines (including IRGs STAT1, OAS1, IFN-β, IFN-γ, IL-2, IL-6, IL-10 and TNF-α) in splenocytes increased linearly with increasing hydrophobicity of the NPs, except for one type of NP with a highly exposed charge which might induce alternate response (Fig. 6C). At a low hydrophobicity degree, hydrophobicity and the cytokines (IL-10 and TNF-α) release levels were found to be positively correlated *in vivo*, whereas such correlation was less evident at a high hydrophobicity degree (Fig. 6D). In a recent study, Kakizawa *et al.* also found that the secretion of cytokine IL-1β from BMDCs and the IFN-γ levels produced by T cells co-cultured with NP-

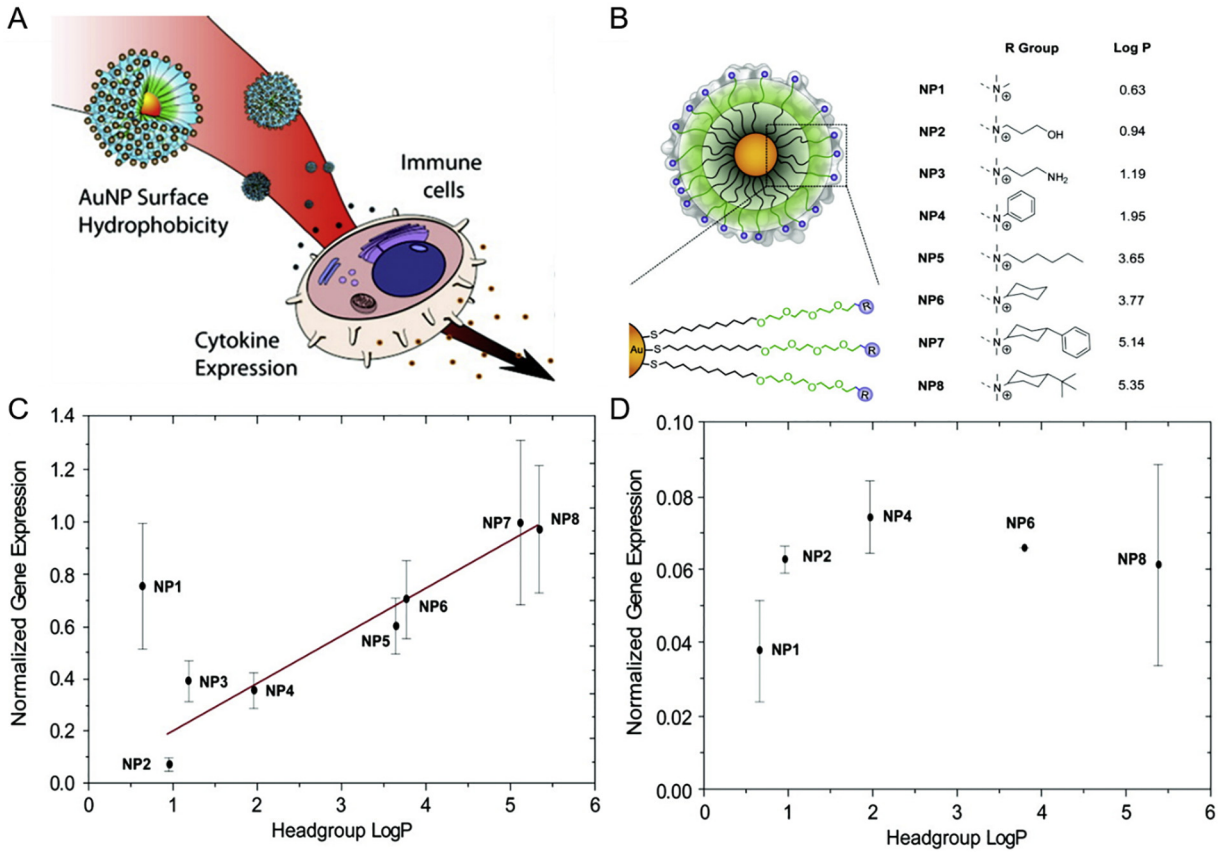

Fig. 6. (A) Effect of hydrophobicity on the immune response of splenocytes. The gene expression profile of a range of cytokines (immunological reporters) was analyzed against the calculated log P of the NP headgroups. (B) Chemical structure of the monolayer-protected 2-nm core diameter gold NPs. Log P represents the calculated hydrophobic values of the headgroups. (C) TFNα *in vitro* gene expression and (D) IL-10 *in vivo* gene expression as a function of the calculated AuNP headgroup log *P* value. The gene expression levels are normalized by dividing the observed response against the values of a positive control (LPS) under the same experimental set. A minimally interacting neutral particle (NP9) was used as a negative control. NPs were used at a concentration of 10 μM for *in vitro* and 5 mg/kg for *in vivo* studies. Data were taken 2 h (*in vitro*) and 1.5 h (*in vivo*) after exposure to AuNPs. Reproduced with permission from [102].

pulsed BMDCs were both positively correlated with NP surface hydrophobicity [82]. The NP systems discussed in this section are summarized in Table 4.

6. Effect of NP rigidity on lymphatic targeting

Compared to other properties, NP rigidity has been less investigated, mainly due to the difficulties in generating NPs with different degree of rigidities while similar other properties. In general, NP rigidity is controlled by tuning the fraction of NP forming materials or using materials with different degree of rigidities in NP preparation. The role of NP rigidity in biodistribution, uptake by APCs and immune response of NPs will be reviewed in this section.

6.1. Effect of NP rigidity on biodistribution

Anselmo *et al.* synthesized PEG based hydrogel NPs with similar particle size and surface charge but different elasticities (elastic moduli: 10 kPa *vs.* 3000 kPa) [109]. After *i.v.* injection, the soft NPs showed higher blood concentration than the hard NPs in the first 4 h, and no difference thereafter. At 30 min, the soft NPs had much higher accumulation in the kidneys, heart, lungs, and brain than the hard NPs. The possible reason is that the higher blood concentration of soft NPs at the short time points may cause the increased retention at the tissues with high blood flow. At 12 h, the soft NPs only showed significantly higher accumulation in the lungs than the hard NPs. In another study, Christensen *et al.* found that the dimethyldioctadecylammonium (DDA)-based liposomes (rigid) had a longer retention time at the site of injection (SOI) than the dimethyldioleoylammonium (DODA)-based liposomes (highly fluidic) after *i.m.* injection, which induced a delayed draining to the dLNs of DDA-based NPs (Fig. 7) [110].

6.2. Effect of NP rigidity on APC uptake

NP rigidity also significantly affect the phagocytosis process. For the PEG based hydrogel NP system mentioned above, the hard NPs showed much higher cellular uptake level than the soft NPs in J774 macrophages and bEnd.3 endothelial cells [109]. Similarly, Palomba *et al.* also demonstrated that the uptake level of hard NPs was up to 5 times higher than that of soft NPs in bone marrow-derived monocytes using discoidal polymeric NPs [111]. This phenomenon may be due to shorter interaction times of soft NPs with the cell membrane compared to that of hard NPs, thus decreasing the likelihood of cell recognition and uptake. The same results were also reported by Hui et al. showing that soft NPs had three times lower uptake than hard NPs in RAW264.7 murine macrophages using liquid-filled silica NPs [112].

6.3. Effect of NP rigidity on immune response

Research investigating the effect of NP rigidity on immune response is still limited. Hard liposomes induced almost 100 times higher level of Th-1 responses than soft liposomes when co-delivered with antigen Ag85B-ESAT-6 upon *i.m.* injection [110]. In addition, hard liposomes tend to form depot at injection site, which continuous attracted APCs and induced high expression level of co-stimulators CD40 and CD86. In contrast, soft liposomes were removed from the injection site quickly,

Table 4
Examples of NPs used to investigate the effect of hydrophobicity on lymphatic targeting.

NP forming materials	Payload/ dye	Main characteri-zations	Immune cells	Animal model	R.A.	Key findings	Ref.
Polyanhydride NPs formed by SA, CPH and CPTEG	*Bacillus anthracis* PA	Four NPs with different hydrophobicity: 20:80 CPTEG:CPH, 50:50 CPH:SA, 50:50 CPTEG:CPH and 20:80 CPH:SA NPs		A/J mice	*s.c.*	20:80 CPTEG:CPH and 50:50 CPH:SA NPs showed slower PA release than 50:50 CPTEG:CPH and 20:80 CPH:SA NPs; Compared with the two CPH:SA polymers, the two amphiphilic polymers CPTEG:CPH were better at preserving the bioactivity and immunogenicity of PA during the fabrication process and in *in vivo* applications.	[97]
PP and PS		Hydrophobicity: PS NPs > PP NPs		Wistar albino rats	*s.c.*	PP NPs showed higher LN accumulation than PS NPs.	[107]
Generation-5 polypropylenimine dendrimer, Gadomer-17 and PAMAM dendrimer		Hydrophobicity: generation-5 polypropylenimine dendrimer and Gadomer-17 > PAMAM dendrimer		Athymic mice	*i.d.*	Generation-5 polypropylenimine dendrimer and Gadomer-17 showed higher axillary LN accumulation than PAMAM dendrimer of similar sizes.	[46]
PGA-g-Phe	OVA	NPs with various grafting degrees of hydrophobic side chains ranging from 43% to 71%	BMDCs	C57BL/6 mice	*s.c.*	BMDC uptake and activation increased with increasing hydrophobicity of the NPs; Cellular immune response increased when the grafting ratio was increased from 43% to 65%, but then decreased when the grafting ratio was increased from 65% to 71%.	[98]
Gold		NPs with different surface functional groups	Splenocytes	Mice	*i.v.*	Cytokine levels in splenocytes increased linearly with increasing hydrophobicity of the NPs; Positive correlations were found between hydrophobicity and the cytokines release levels at a low hydrophobicity degree *in vivo*, whereas such correlation was less evident at a high hydrophobicity degree.	[102]
Silica NPs modified with PAA		NPs with different hydrophobicities	BMDCs and OT-I T cells			The secretion of cytokine IL-1β from BMDCs and the IFN-γ levels produced by T cells co-cultured with NP-pulsed BMDCs were both positively correlated with NP surface hydrophobicity.	[82]

SA: sebacic anhydride; CPH: 1,6-bis(pcarboxyphenoxy) hexane; CPTEG: 1,8-bis(pcarboxyphenoxy)-3,6-dioxaoctane; PP: PLGA-PMA:PLA-PEG; PS: polystyrene; PAMAM: poly(amido-amine); PGA-g-Phe: poly(g-glutamic acid)-*graft*-Lphenylalanine ethyl ester; PAA: poly(amino acid); PA: protective antigen; BMDCs: bone marrow-derived dendritic cells; R.A.: route of administration; *s.c.*: subcutaneous; *i.d.*: intradermal; *i.v.*: intravenous; Ref.: reference.

which induced a lower up-regulation of CD40 and CD86 of adjuvant positive APCs. More studies are needed in the future to understand the relationship between NP rigidity and immune response *in vivo*. The NP systems discussed in this section are summarized in Table 5.

7. Effect of NP surface-conjugated ligand on lymphatic targeting

Active targeting by decorating targeting ligands on the surface of NPs is one of the effective strategies to modulate immune response at the single-cell level [1]. Using this strategy, loaded immunomodulation reagents can be delivered to a subset of immune cells specifically to reduce the non-specific toxicity and enhance the immune response. In this section, various NP systems for macrophage, DC and T cell active targeting will be reviewed.

7.1. Effect of NP surface-conjugated ligand on macrophage and DC targeting

Macrophages are a type of phagocytes that can be found essentially in all tissues in the body. These cells differentiate from immature monocytes and play an important role in nonspecific immune defense by engulfing and digesting foreign substances, cell debris and pathogens. In addition, they are involved in initiating adaptive immunity by

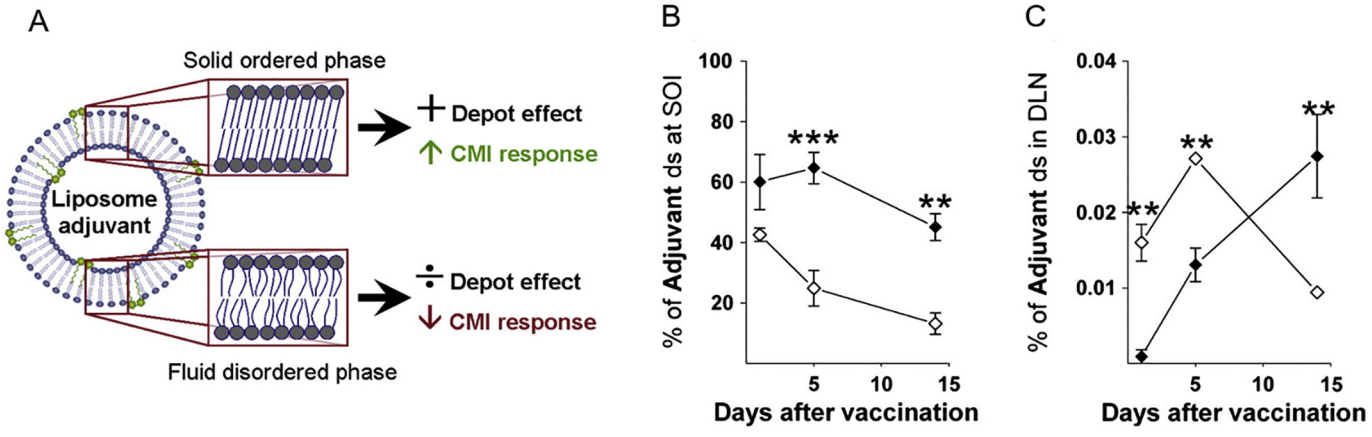

Fig. 7. NP rigidity plays and important role in biodistribution and ability to activate an immune response. (A) Liposome composition impacts lipid structure organization and fluidity and its ability to ensure that Ag + APCs are activated to prime, polarize and mature cell-mediated immune (CMI) responses. Bioavailability of the adjuvant is increased at site of injection with decreased fluidity of the liposomes, resulting in a delayed draining of the adjuvant to the LNs. Mice were vaccinated through the *i.m.* route with I^{125}-Ag85B-ESAT-6 co-administered with either H^3-DODA/TDB (◊) or H^3-DDA/TDB (♦). Site of injection (SOI) and local dLN from mice were isolated at days 1, 5 and 14 after vaccination and the percentage of total administered adjuvant dose present at the two locations determined by radiation quantification: (B) adjuvant at SOI and (C) adjuvant in dLN, Three mice per group (mean ± SEM), representative of two independent experiments. ** $p < 0.01$, *** $p < 0.001$. Reproduced with permission from [110].

Table 5
Examples of NPs used to investigate the effect of rigidity on lymphatic targeting.

NP forming materials	Payload/dye	Main characteri-zations	Immune cells	Animal model	R.A.	Key findings	Ref.
PEG based hydrogel NPs	*Bacillus anthracis* PA	Rigidity: elastic moduli: 10 kPa and 3000 kPa	J774	BALB/c mice	*i.v.*	Soft NPs showed higher blood concentration than the hard NPs in the first 4 h; At 30 min, the soft NPs had much higher accumulation in the kidneys, heart, lungs, and brain than the hard NPs; At 12 h, the soft NPs only showed significantly higher accumulation in the lungs than the hard NPs; Hard NPs showed much higher cellular uptake level than the soft NPs in J774 macrophages.	[109]
Liposomes formed by DDA or DODA	TDB	Rigidity: DDA-based liposomes >DODA-based liposomes		C57BL/6 mice	*i.m.*	DDA-based liposomes had a longer retention time at the site of injection (SOI) than the DODA-based liposomes, which induced a delayed draining to the dLNs of DDA-based NPs; DDA-based liposomes induced almost 100 times higher level of Th-1 responses than DODA-based liposomes when co-delivered with antigen Ag85B-ESAT-6.	[110]
Discoidal polymeric NPs formed by PLGA and PEG-DA	Rhodamine B	Rigidity: elastic moduli ranging from 100 kPa to 10 mPa	RAW264.7 and BMDCs			The uptake level of hard NPs was up to 5 times higher than that of soft NPs in BMDCs.	[111]
Liquid-filled silica NPs	Dil	Rigidity: elastic moduli ranging from 704 kPa to 9.7 GPa	RAW264.7			Soft NPs had three times lower uptake than hard NPs.	[112]

PEG: polyethylene glycol; DDA: imethyldioctadecylammonium; DODA: dimethyldioleoylammonium; PLGA: poly(lactic-co-glycolic acid); PEG-DA: poly(ethylene glycol) diacrylate; PA: protective antigen; TDB: Trehalose-6,6-dibehenate; BMDCs: bone marrow-derived dendritic cells; R.A.: route of administration; *i.v.*: intravenous; *i.m.*: intramuscular; Ref.: reference.

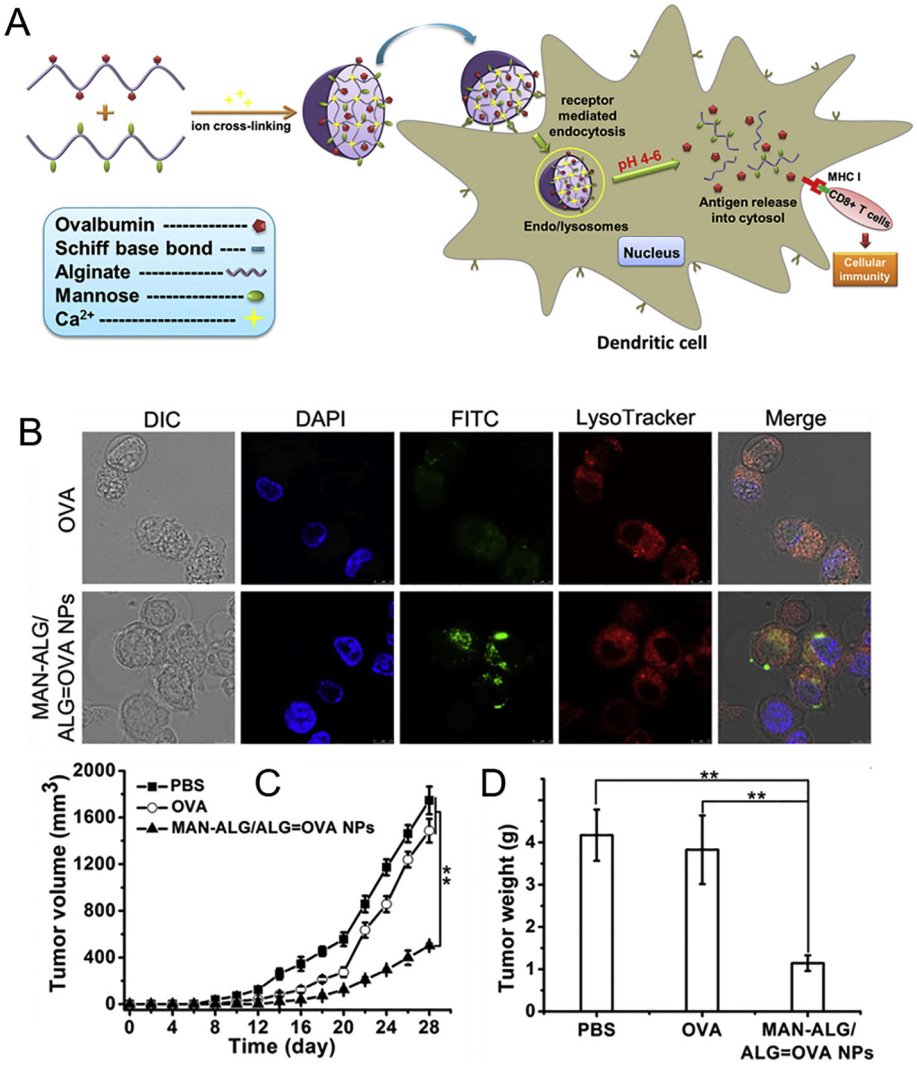

Fig. 8. "Easy-to-adopt" strategy to enhance the immune response using functionalized alginate NPs. (A) Alginate NPs were fabricated using a pH sensitive Schiff base linkage that allows for release of the antigens of interest into DC cytoplasm and antigen presentation *via* MHC. (B) Confocal microscope images of DCs after incubation with free OVA and mannose targeted (MAN-ALG/ALG = OVA) NPs. The bar scale indicates 75 μm. (C) Tumor volume and (D) Tumor weight during the total immunotherapy course using free OVA or mannose targeted NPs in mice bearing E.G7 tumors. The statistical significance in difference was analyzed using student's *t*-Test: *$p < 0.05$ and **$p < 0.01$. Reproduced with permission from [124].

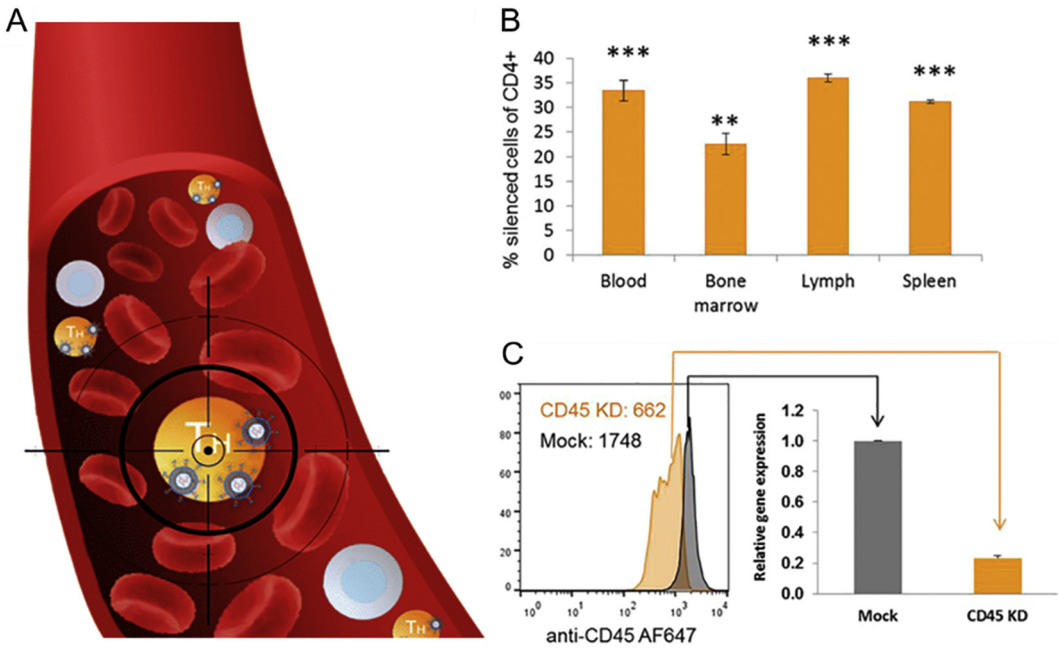

Fig. 9. Modulation of T cell function *via* deliver of siRNAs to CD4+ T cells using targeted lipid NPs (tLNPs). (A) The tLNPs were surface-functionalized with anti-CD4 monoclonal antibody to enable efficacious and specific delivery of the siRNAs specifically to CD4+ T lymphocytes. Silencing of CD45 in $CD4^+$ T cells at the protein (B) and the mRNA (C) level. Five days after administration of tLNP carrying siCD45, spleen, LNs, bone marrow, and blood lymphocytes were isolated and analyzed by FACS. Error bars represent mean ± SD, n = 5 mice/group, ***$p < 0.0005$, **$p < 0.005$ are compared to mock treated sample. mRNA was isolated, and CD45 mRNA levels in the spleen were tested by quantitative polymerase chain reaction. All values are normalized to murine PPIB gene expression (endogenous control). Reproduced with permission [145].

presenting antigens to lymphocytes and secreting cytokines. Macrophages are also critical regulators of the inflammatory process and can be sub-classified into M1 macrophages that are pro-inflammatory and M2 macrophages that are anti-inflammatory [113]. The balance of M1 and M2 macrophages plays a vital role in the development of various diseases such as inflammatory bowel disease, rheumatoid arthritis, atherosclerosis, diabetes and cancer. DCs are key APCs and play multiple important roles in initiating and shaping the adoptive immune response depending upon their subtype and tissue location. The main function of the conventional dendritic cells (cDCs) is to process and present antigen to T cells, whereas pDCs are responsible for mass-production of Type 1 interferons upon viral infection. Targeted NPs with surface modifications have shown great promise in the ability to specifically deliver immunomodulatory compounds and antigens to macrophages and DCs.

The mannose receptor (CD206) is a C-type lectin that is primarily expressed on the surface of mature macrophages and many DC populations [114]. Thus, mannose has been widely employed as a simple but effective ligand for targeting NPs to macrophages and DCs. Tumor-

Table 6
Summary of NPs for macrophage, DC and T cell active targeting.

Immune Cell Targeting	Targeting Ligand	R.A.	NP Forming Materials	Ref.
Macrophage targeting	Mannose	*i.v.*	HA coated MnO_2 NPs	[116]
		i.v.	PEG sheddable PLGA NPs	[119–121]
		i.m., *i.p.* and intubation	Poly(BMA-*co*-PAA-*co*-DMAEMA)-*b*-poly(DMAEMA)-*b*-poly(AzEMA)	[117,118]
	HA	*i.v.*	Poly(DEGMA-*co*-OEGMA) grafted HA	[149]
	F4/80 antibody fragments	*i.p.*	HA modified PEI	[126–129]
		i.p.	Cholanic acid modified HA	[130]
		oral	PLA-PEG	[131]
DC targeting	Mannose	–	Poly(HPMA)-*b*-poly(LMA)	[122]
		s.c.	CS	[123]
		i.v.	Alginate	[124]
		–	PEGylated hydroxyethyl starch	[125]
	Anti-DEC-205 antibody	*i.v.*	Dextran coated iron oxide microcrystals	[132]
	Anti-CD209 antibody	–	PVA coated gold NPs	[133]
	Anti-CD40 antibody and anti-CD11c antibody	*s.c.*	PLGA	[134]
T-cell targeting	Anti-CD3 antibody	–	PEG-*g*-PEI with SPION	[139]
		i.v.	PEG-SPION	[141]
	CD4 targeting peptides	–	Lipid NPs	[143,144]
		i.v.	Lipid NPs	[145]
	Integrin targeting antibody	*i.v.*	HA coated lipid NPs	[147,148]

HA: hyaluronic acid; R.A.: route of administration; *i.v.*: intravenous; *i.m.*: intramuscular; *i.p.*: intraperitoneal; *s.c.*: subcutaneous; PEG: polyethylene glycol; PLGA: poly(lactic-*co*-glycolic acid); BMA: butyl methacrylate; PAA: 2-propylacrylic acid; DMAEMA: 2-dimethyl aminoethyl methacrylate; AzEMA: 2-azidoethyl methacrylate; DEGMA: di(ethylene glycol) methacrylate; OEGMA: oligo(ethylene glycol) methacrylate; PEI: polyethyleneimine; HPMA: N-[2-hydroxypropyl] methacrylamide; LMA: lauryl methacrylate; CS: chitosan; PVA: polyvinyl alcohol; SPION: superparamagnetic iron oxide nanoparticles. Ref.: reference.

Table 7
NPs currently tested for immunotherapy in clinical trials.

Products	NP Systems	NP Properties	Payloads	Indications	Identifier (Phase)	R.A.	Ref.
CAF01	Liposomes formed by DDA and TDB	Size: 50-5000 nm Charge: positive Shape: primarily unilamellar		Tuberculosis	NCT00922363 (Ph 1, completed)	*i.m.*	[151]
CCS/C	Liposomes formed by CCS and cholesterol	Size: 100-3000 nm Charge: positive Shape: mixture of uni-, oligo- and multi-lamellar vesicles	Hemagglutinin	Influenza	NCT00915187 (Ph 2, completed)	*i.m.*	[152]
AS01	Liposomes formed by DMPC, DMPG, cholesterol and a synthetic MPL (3D-PHAD®)	Distribution: poly-dispersed Shape: unilamellar	MPL and QS21	Malaria	NCT03824236 (Ph2, ongoing)	*i.m.*	[153]
				HIV	NCT03368053 (Ph1, completed)		
				Tuberculosis	NCT01755598 (Ph 2, completed)		
DPX-0907	DepoVax™(DPX): Liposomes formed by DOPC and cholesterol	Size: ~120 nm Charge: positive	Seven tumor-specific HLA-A2-restricted peptides, a universal T Helper peptide (A16L), and a polynucleotide adjuvant	Ovarian, breast or prostate cancer	NCT01095848 (Ph 1, completed)	*s.c.*	[154,155]
DPX-Survivac			Survivin epitopes and a polynucleotide adjuvant	Advanced stage ovarian, fallopian or peritoneal cancer	NCT01416038 (Ph 1, completed)	*s.c.*	[156,157]
				Recurrent ovarian cancers	NCT02785250 (Ph 1, ongoing)		
				Recurrent survivin-expressing diffuse large B-cell lymphoma	NCT02323230 (Ph 2, ongoing)		
				Advanced stage ovarian, fallopian or peritoneal cancer	NCT03332576 (Ph 1, ongoing)		
				Advanced stage ovarian, fallopian or peritoneal cancer	NCT03029403 (Ph 2, ongoing)		
				Recurrent diffuse large B-cell lymphoma	NCT03349450 (Ph 2, ongoing)		
				Advanced stage ovarian, hepatocellular, non-small cell lung or bladder cancers	NCT03836352 (Ph 2, ongoing)		
DPX-RSV(A)			A synthetic Respiratory Syncytial Virus small hydrophobic glycoprotein antigen	Respiratory Syncytial Virus	NCT02472548 (Ph 1, active)	*i.m.*	[158]
Lipo-MERIT	Lipopolexes formed by DOTMA/DOPE liposomes and mRNA	Size: 200-320 nm Charge: negative	Four mRNA encoding melanoma antigens	Melanoma	NCT02410733 (Ph1, ongoing)	*i.v.*	[86]
BLP25	Liposomes formed by DMPG, DPPC and cholesterol	Size: ~800 nm Charge: positive	Tecemotide and MPL	Multiple myeloma	NCT01094548 (Ph 2, completed)	*s.c.*	[159–162]
				Colon or rectum cancer	NCT01462513 (Ph 2, completed)		
				Prostate cancer	NCT01496131 (Ph 2, completed)		
				Non-small cell lung cancer	NCT00157196 (Ph 2, completed)		
				Rectal cancer	NCT01507103 (Ph 2, completed)		
				Stage III non-small cell lung cancer	NCT00960115 (Ph 1, 2, completed)		
				Stage III non-small cell lung cancer	NCT00828009 (Ph 2, ongoing)		

(continued on next page)

Table 7 (*continued*)

Products	NP Systems	NP Properties	Payloads	Indications	Identifier (Phase)	R.A.	Ref.
				non-small cell lung cancer	NCT00157209 (Ph 2, completed)		
				Stage III non-small cell lung cancer	NCT00409188 (Ph 3, completed)		
Lipovaxin-MM	Liposomes formed by human melanoma cell MM200 membrane and POPC/Ni-3NTA-DTDA liposomes	Targeting ligand: DC targeting antibody DMS5000	IFN-γ	Melanoma	NCT01052142 (Ph 1, completed)	*i.v.*	[163]

DDA: dimethyldioctadecylammonium; TDB: α,α'-trehalose 6,6'-dibehenate; CCS: ceramide carbamoyl-spermine; DMPC: dipalmitoylphosphatidylcholine; DMPG: dimyristoyl phosphatidylglycerol; DOPC: dioleoylglycero phosphocholine; DOTMA: 1,2-di-O-octadecenyl-3-trimethylammonium propane; DOPE: dioleoylphosphatidylethanolamine; DPPC:

associated macrophage (TAM) are a population of immune cells present in the microenvironment of solid tumors and play a key role in inducing immunosuppressive microenvironment [115]. Mannose modified NPs have been extensively employed as carrier systems for immunomodulatory compound delivery to polarize TAM from M2 pro-tumor phenotype to M1 anti-tumor phenotype for cancer immunotherapy [116–118]. However, one issue of these NP systems is that the uptake by normal macrophages may cause toxicity. To address this issue, Zhu *et al.* designed and synthesized PEG-sheddable and mannose-modified PLGA NPs [119]. These NPs had low uptake by the normal macrophages in the mononuclear phagocyte system (MPS) organs due to the presence of PEG at neutral pH during blood circulation, while specifically target TAM by mannose receptor recognition after pH-sensitive PEG cleavage in the acidic tumor microenvironment [119]. Delivery of DOX using this NP system showed higher tumor accumulation, TAM depletion and tumor inhibition with no toxicity to macrophages in the MPS compared to free DOX in both murine melanoma B16-F10 xenograft tumor model and orthotopic M-Wnt triple-negative mammary tumor model [120,121]. Mannose modified NPs have also been used for the delivery of immunomodulatory compound to DCs for DC stimulation [104]. In addition, these NP systems can be employed for specifically delivery of antigen to DCs for cancer immunotherapy. For example, Shi *et al.* prepared mannose-modified chitosan NPs to deliver B16 melanoma cancer cell lysates for specific DC targeting, which showed strong protective and therapeutic effects in melanoma tumor model [123]. The same group also generated pH-sensitive mannose-functionalized alginate NPs for a model antigen OVA delivery [124]. These NPs showed strong targeting and activation effect in BMDCs *in vitro* (Fig. 8A). DC targeting, T cell activation and the therapeutic effect of this platform was further confirmed in an *in vivo* E.G7 lymphoma tumor model (Fig. 8B and C) [124]. The targeting effect of the surface ligand-modified NPs may be affected by the protein corona after administration. However, in a study performed by Kang *et al.*, they demonstrated that mannose-modified PEGylated hydroxyethyl starch NPs showed lower overall protein adsorption and higher affinity to mature DCs generated from human peripheral blood mononuclear cells when compared with hydroxyethyl starch NPs and PEGylated hydroxyethyl starch NPs in the presence of human plasma [125].

The HA receptor CD44 is known to be overexpressed on the membrane of macrophages. The Amiji group synthesized HA- modified PEI to deliver genetic payloads to macrophages for modulating macrophage functional polarity. They successfully applied this system to deliver IL-4 and IL-10 plasmid DNA, microRNA-223 and TNF-α siRNA to macrophages [126–128]. More recently, they used this system to deliver microRNA-125b to repolarize TAM in a genetically-engineered non-small cell lung cancer model (Fig. 8) [129]. In another example, Beldman *et al.* prepared HA NPs by reacting amine-functionalized oligomeric HA with cholinic ester to target plaque-associated macrophages for atherosclerosis treatment. These NPs showed higher accumulation in aortic macrophages than normal tissue macrophages, and also had atheroprotective effects by decreasing the population of plaque-associated macrophages in atherosclerotic mice [130]. NPs modified with F4/80 antibody fragments can also target macrophages. Laroui *et al.* conjugated F4/80 antibody Fab fragment onto the surface of PLA-PEG NPs for TNF-α siRNA delivery [131]. These NPs demonstrated enhanced targeting effect in RAW264.7 cells *in vitro*. In mice with colitis induced by 3% dextran sodium sulfate, oral treatment with targeted NPs in chitosan/alginate hydrogel had a better therapeutic effect than untargeted NPs in the same hydrogel [131].

DEC-205 (CD205) is an C-type lectin receptor exclusively expressed on lymphoid tissue DCs, and not on other peripheral blood mononuclear cells [114]. Shen *et al.* generated NP surface-conjugated with CpG-oligonucleotides (CpG-ODNs), OVA and anti-DEC-205 antibody for CD8α + DC targeting [132]. These trifunctional NPs showed strong antitumor effect and prolonged the survival rate in mice bearing B16-OVA tumor [132]. Dendritic Cell-Specific Intercellular adhesion molecule-3-Grabbing Non-integrin (DC-SIGN or CD209) is another lectin receptor expressed specifically by immature DCs in peripheral tissue and mature DCs in lymphoid tissues [114]. Fytianos *et al.* investigated the aerosol delivery efficiency of DC-SIGN antibody-modified gold NPs in a 3D lung cellular model [133]. The DC-SIGN antibody-modified NPs showed higher DC targeting and significantly upregulated MHC-II expression level in DCs when compared with unmodified NPs [133]. The DC targeting effect of three antibodies binding CD40, DEC-205 or CD11c was compared by coupling them on the surface of PLGA NPs [134]. CD40 is a TNF-α family receptor that induces DC activation after binding with its specific ligand, while CD11c, an integrin receptor, and DEC-205, do not induce DC activation after binding with their respective ligands. OVA was co-loaded with Toll like receptor 3 and 7/8 agonists (polyinosinic:polycytidylic acid and resiquimod, respectively) into the NPs. BMDCs showed stronger binding to and internalization of all three of the targeted NPs *in vitro* compared to untargeted NPs. Interestingly, the CD40-targeted NPs were more efficiently internalized by BMDCs than DEC-205- or CD11c-targeted NPs. However, DC activation and T cell stimulation by the three targeted NPs were comparable, which were significant higher than the untargeted NPs both *in vitro* and *in vivo* [134].

7.2. Effect of NP surface-conjugated ligand on T-cell targeting

T lymphocytes play a critical role in the adaptive immune response, and they are involved in clearing various infectious diseases, cancers and autoimmune diseases [135,136]. NPs modified with surface targeting ligands have shown great promise for T lymphocytes targeting for both drug/gene delivery and *in vivo* imaging [135,137,138].

One of the most extensively used T cell targets is the CD3 receptor expressed on the surface of T cells [138–142]. Anti-CD3 single chain antibody (scAbCD3) has been used for superparamagnetic iron oxide

nanoparticles (SPIONs) surface modification as DNA carriers for T cell imaging and immunosuppression [139]. Chen *et al.* conjugated monoclonal anti-CD3 antibody on the surface of the carboxylated-PEG-SPION (IOPC) for *in vivo* T cells labelling and trafficking [141]. These NPs showed strong T cells labelling ability both *in vitro* and *in vivo*. The T cells labeled by these NPs were effectively imaged by MRI in a rodent collagen-induced arthritis (CIA) model.

The CD4+ T helper cells and their expressed cytokines are vital to modulating the immune system [136]. To influence the activity of CD4 + T cells and subsequent polarization of the systemic immune response, various CD4+ targeting NPs have been developed. Endsley *et al.* first identified two peptides which could provide specific targeting to HIV-infected CD4+ host cell when conjugated on the surface of lipid NPs [143]. In a subsequent study, they demonstrated that NPs modified with the two peptides could effectively deliver an HIV anti-retroviral protease inhibitor, indinavir, into HIV-infected CD4+ host cells with enhanced anti-viral activities when compared with unmodified NPs and free indinavir [144]. In another example, CD4+ T cell-targeting lipid nanoparticles (tLNPs) with surface conjugated anti-CD4 antibody were prepared to deliver siRNA to CD4+ T cells for immunomodulation [145]. CD45 siRNA was used in this study as a model gene since CD45 is a pan leukocyte marker which can be used for testing specific silencing in different leukocyte subsets. CD4+ T cells located in the blood circulation, bone marrow, spleen and inguinal LNs were selectively targeted and silenced by these NPs after *i.v.* injection in mice (Fig. 9).

Another specific T-lymphocyte target are leukocyte-specific integrins [146]. It has been shown that antibody-protamine fusion proteins targeting the human integrin lymphocyte function-associated antigen-1 (LFA-1) can specifically deliver siRNA to leukocytes and induce gene silencing both *in vitro* and *in vivo* [146]. In a subsequent study, antibodies to β7 integrin were conjugated to the surface of targeted stabilized NPs for the delivery of cyclin D1 siRNA to leukocytes [147]. These NPs induced strong cyclin D1 silencing effect in leukocytes and significantly reduced the intestinal inflammation in colitis-induced mice after systemic injection. The same tsNPs system was used for HIV infection treatment by replacing the β7 integrin antibody with the ligand of LFA-1 [148]. Humanized mice treated with anti-CCR5 siRNA-loaded targeted NPs showed long-term leukocyte-specific gene silencing (10 days) and enhanced resistance to HIV challenges.

The NPs systems with targeting ligands on the surface for macrophage, DC and T cell active targeting discussed in this section are summarized in Table 6.

8. Conclusion and future perspectives

NPs provide a versatile platform for antigen and adjuvant delivery for disease prevention and treatment. Various physicochemical properties of the NPs including particle size, shape, surface charge, hydrophobicity, rigidity and surface targeting ligand significantly influence the biodistribution, LN targeting, antigen release, APC interaction and immune response *in vivo*. Through fine-tuning these parameters, enhanced immune response and decreased toxicity can be achieved. It is important to point out that aside from the chemical nature of the NP forming materials, the relationship between these design parameters and immune responses is also likely dependent on the route of administration. There are several general rules in NP design for specific lymphatic targeting. For example, to achieve effective dLN targeting, NPs with small size and negative charge through *s.c.* or *i.d.* injection are preferred. Spherical NPs with high hydrophobicity and high rigidity tend to have higher APC uptake and stronger APC activation effect than worm NPs with low hydrophobicity and low rigidity. In addition, NPs with small size induce stronger Th1 immune response than NPs with large size. Various targeting ligands can be used for NP surface modification for specific immune cell targeting. Several NP formulations are currently under clinical trials for infection disease prevention and cancer treatment (Table 7). Most of these formulations are liposomes formed by cationic lipids and loaded with antigens and adjuvants, with positive surface charge. In one exception, Lipo-MERIT are lipopolexes complexed by cationic liposomes and four mRNA sequences encoding melanoma antigens at charge ratio 1.3 to 2 with overall negative charge. Lipovaxin-MM are active targeted NPs with DMS5000 antibody on the surface for DC targeting. CAF01 and AS01 are two NP systems served as adjuvants and combined with other vaccine systems for infection disease protections.

To further probing the detailed structure-property-function relationship of the nanovaccines and to advance their clinical translation, generating NP vaccines with well-defined physicochemical properties using a scalable and reproducible process is critical. Yet, encapsulating protein antigens or antigen-encoding nucleic acids into size and shape-controlled NPs represents a great challenge. Recently our group has developed a scalable NP preparation platform (FNC) for DNA, protein and peptide therapeutics delivery [37–42]. By tuning the formulation conditions, the physicochemical properties of the NPs can be fine-tuned. With this platform, we have generated NPs for the co-delivery of the subunit VP1 protein antigen of the enterovirus 71 (EV71), which is the primary cause for hand-foot-mouth disease, with TNF-α or CpG-ODN as an adjuvant [41]. These NPs have smaller particle size, narrower size distribution, higher loading level and stronger LN accumulation. Most importantly, these NPs provided effective protection against lethal viral challenge in mouse models with both passive and active immunization, a finding comparable to the effect elicited by a currently approved inactivated viral vaccine [41]. This platform has great potential for manufacturing NPs with specific properties for antigen and adjuvant delivery, with the ability of rapid clinical translation in the future. Platform with high reproducibility and manufacturability and the ability for NP composition control will serve as an important toolset for studying NP physicochemical parameters and increase the likelihood of bench to bedside translation of these NP vaccines and immunotherapeutics.

Tailored NP design with optimized physicochemical parameters will have the potential to improve the treatment outcomes of many immunotherapies. Understanding the mechanism of action by which NPs with different properties influence lymphatic targeting will be critical to rational design of NP systems for the delivery of vaccines and immunotherapeutic agents. In addition, demonstrating whether a specific lymphatic targeting mechanism for NPs observed in rodents translates into higher species including non-human primates and humans will be paramount to realize the potential of NP carriers in immunotherapy. In this regard, the effect of protein corona formed on the surface of NPs after administration in different species also needs to be considered in NP design for immunotherapy [94,95]. Besides those physicochemical properties discussed above, the release profile of the immunomodulatory agents from the NPs and the stability of NPs may modulate the lymphatic system targeting of NPs. Combination therapy using multiple immunomodulation agents will continue to be explored in immunotherapy [150]. Although many NPs have the capacity for co-delivery of multiple reagents, using a set of NPs designed for different functionalities may be preferred for targeting different organs or cells or achieving different release profiles. In addition, stimuli-responsive NPs that can release payloads upon triggers specific at the target immune tissue, cells, or subcellular compartment will further improve the targeted delivery efficiency, decrease the side effects, and enhance immunotherapeutic outcomes.

Declaration of Competing Interest

This article was prepared while May Tun Saung was employed at Johns Hopkins University. The opinions expressed in this article are the author's own and do not reflect the view of the Food and Drug Administration, the Department of Health and Human Services, or the United States government. There are no conflicts to declare by all other authors.

Acknowledgements

This work was supported by the National Institutes of Health (R21 5R21AI133533), the National Science Foundation (GRFP DGE1746891), and a AstraZeneca MedImmune Partnership Grant.

References

[1] D.J. Irvine, M.C. Hanson, K. Rakhra, T. Tokatlian, Synthetic nanoparticles for vaccines and immunotherapy, Chem. Rev. 115 (2015) 11109–11146.
[2] H. Yue, G. Ma, Polymeric micro/nanoparticles: Particle design and potential vaccine delivery applications, Vaccine 33 (2015) 5927–5936.
[3] W.C. Koff, D.R. Burton, P.R. Johnson, B.D. Walker, C.R. King, G.J. Nabel, R. Ahmed, M.K. Bhan, S.A. Plotkin, Accelerating next-generation vaccine development for global disease prevention, Science 340 (2013), 1232910.
[4] J.A. Berzofsky, J.D. Ahlers, I.M. Belyakov, Strategies for designing and optimizing new generation vaccines, Nat. Rev. Immunol. 1 (2001) 209–219.
[5] R. Rappuoli, M. Pizza, G. Del Giudice, E. De Gregorio, Vaccines, new opportunities for a new society, Proc. Natl. Acad. Sci. U. S. A. 111 (2014) 12288–12293.
[6] A.M. Harandi, D. Medaglini, R.J. Shattock, Vaccine adjuvants: a priority for vaccine research, Vaccine 28 (2010) 2363–2366.
[7] L. Jeanbart, M.A. Swartz, Engineering opportunities in cancer immunotherapy, Proc. Natl. Acad. Sci. 112 (2015) 14467–14472.
[8] K. Shao, S. Singha, X. Clemente-Casares, S. Tsai, Y. Yang, P. Santamaria, Nanoparticle-based immunotherapy for cancer, ACS Nano 9 (2015) 16–30.
[9] D.M. Pardoll, The blockade of immune checkpoints in cancer immunotherapy, Nat. Rev. Cancer 12 (2012) 252–264.
[10] A. Bertrand, M. Kostine, T. Barnetche, M.E. Truchetet, T. Schaeverbeke, Immune related adverse events associated with anti-CTLA-4 antibodies: systematic review and meta-analysis, BMC Med. 13 (2015) 211.
[11] W.J. Cliff, P.A. Nicoll, Structure and function of lymphatic vessels of the bat's wing, Q. J. Exp. Physiol. Cogn. Med. Sci. 55 (1970) 112–121.
[12] A.E. Taylor, Capillary fluid filtration: starling forces and lymph flow, Circ. Res. 49 (1981) 557–575.
[13] N.L. Trevaskis, L.M. Kaminskas, C.J.H. Porter, From sewer to saviour-targeting the lymphatic system to promote drug exposure and activity, Nat. Rev. Drug Discov. 14 (2015) 781–803.
[14] U.H. Von Andrian, T.R. Mempel, Homing and cellular traffic in lymph nodes, Nat. Rev. Immunol. 3 (2003) 867–878.
[15] K. Hanatani, K. Takada, N. Yoshida, M. Nakasuji, Y. Morishita, K. Yasako, T. Fujita, A. Yamamoto, S. Muranishi, Molecular weight-dependent lymphatic transfer of fluorescein isothiocyanate-labeled dextrans after intrapulmonary administration and effects of various absorption enhancers on the lymphatic transfer of drugs in rats, J. Drug Target. 3 (1995) 263–271.
[16] G.J. Randolph, V. Angeli, M.A. Swartz, Dendritic-cell trafficking to lymph nodes through lymphatic vessels, Nat. Rev. Immunol. 5 (2005) 617–628.
[17] L.G. Griffith, M.A. Swartz, Capturing complex 3D tissue physiology in vitro, Nat. Rev. Mol. Cell Biol. 7 (2006) 211–224.
[18] L.M. Kaminskas, C.J.H. Porter, Targeting the lymphatics using dendritic polymers (dendrimers), Adv. Drug Deliv. Rev. 63 (2011) 890–900.
[19] N.L. Trevaskis, L.M. Kaminskas, C.J. Porter, From sewer to saviour - targeting the lymphatic system to promote drug exposure and activity, Nat. Rev. Drug Discov. 14 (2015) 781–803.
[20] S.T. Reddy, A. Rehor, H.G. Schmoekel, J.A. Hubbell, M.A. Swartz, In vivo targeting of dendritic cells in lymph nodes with poly(propylene sulfide) nanoparticles, J. Control. Release 112 (2006) 26–34.
[21] J.I. Andorko, J.M. Gammon, L.H. Tostanoski, Q. Zeng, C.M. Jewell, Targeted Programming of the Lymph Node Environment Causes Evolution of Local and Systemic Immunity, Cell. Mol. Bioeng. 9 (2016) 418–432.
[22] L.H. Tostanoski, Y.C. Chiu, J.M. Gammon, T. Simon, J.I. Andorko, J.S. Bromberg, C.M. Jewell, Reprogramming the local lymph node microenvironment promotes tolerance that is systemic and antigen specific, Cell Rep. 16 (2016) 2940–2952.
[23] R.H. Xu, M. Fang, A. Klein-Szanto, L.J. Sigal, Memory CD8+ T cells are gatekeepers of the lymph node draining the site of viral infection, Proc. Natl. Acad. Sci. U. S. A. 104 (2007) 10992–10997.
[24] I. Moran, A. Nguyen, W.H. Khoo, D. Butt, K. Bourne, C. Young, J.R. Hermes, M. Biro, G. Gracie, C.S. Ma, C.M.L. Munier, F. Luciani, J. Zaunders, A. Parker, A.D. Kelleher, S.G. Tangye, P.I. Croucher, R. Brink, M.N. Read, T.G. Phan, Memory B cells are reactivated in subcapsular proliferative foci of lymph nodes, Nat. Commun. 9 (2018) 1–14.
[25] D. Suan, A. Nguyen, I. Moran, K. Bourne, J.R. Hermes, M. Arshi, H.R. Hampton, M. Tomura, Y. Miwa, A.D. Kelleher, W. Kaplan, E.K. Deenick, S.G. Tangye, R. Brink, T. Chtanova, T.G. Phan, T follicular helper cells have distinct modes of migration and molecular signatures in naive and memory immune responses, Immunity. 42 (2015) 704–718.
[26] X. Zhou, R. Liu, S. Qin, R. Yu, Y. Fu, Current status and future directions of nanoparticulate strategy for cancer immunotherapy, Curr. Drug Metab. 17 (2016) 755–762.
[27] E. Torres-Sangiao, A.M. Holban, M.C. Gestal, Advanced nanobiomaterials: vaccines, diagnosis and treatment of infectious diseases, Molecules. 21 (2016).
[28] W. Song, L. Shen, Y. Wang, Q. Liu, T.J. Goodwin, J. Li, O. Dorosheva, T. Liu, R. Liu, L. Huang, Synergistic and low adverse effect cancer immunotherapy by immunogenic chemotherapy and locally expressed PD-L1 trap, Nat. Commun. 9 (2018).
[29] E.F. Craparo, M.L. Bondi, Application of polymeric nanoparticles in immunotherapy, Curr. Opin. Allergy Clin. Immunol. 12 (2012) 658–664.
[30] S. Cai, Q. Yang, T.R. Bagby, M.L. Forrest, Lymphatic drug delivery using engineered liposomes and solid lipid nanoparticles, Adv. Drug Deliv. Rev. 63 (2011) 901–908.
[31] Z. Amoozgar, M.S. Goldberg, Targeting myeloid cells using nanoparticles to improve cancer immunotherapy, Adv. Drug Deliv. Rev. 91 (2015) 38–51.
[32] S.T. Reddy, A.J. Van Der Vlies, E. Simeoni, V. Angeli, G.J. Randolph, C.P. O'Neil, L.K. Lee, M.A. Swartz, J.A. Hubbell, Exploiting lymphatic transport and complement activation in nanoparticle vaccines, Nat. Biotechnol. 25 (2007) 1159–1164.
[33] C.A. Fromen, G.R. Robbins, T.W. Shen, M.P. Kai, J.P.Y. Ting, J.M. DeSimone, Controlled analysis of nanoparticle charge on mucosal and systemic antibody responses following pulmonary immunization, Proc. Natl. Acad. Sci. 112 (2014) 488–493.
[34] C. Wu, M.E. Muroski, J. Miska, C. Lee-Chang, Y. Shen, A. Rashidi, P. Zhang, T. Xiao, Y. Han, A. Lopez-Rosas, Y. Cheng, M.S. Lesniak, Repolarization of myeloid derived suppressor cells via magnetic nanoparticles to promote radiotherapy for glioma treatment, Nanomedicine 16 (2019) 126–137.
[35] G.P. Howard, G. Verma, X. Ke, W.M. Thayer, T. Hamerly, V.K. Baxter, J.E. Lee, R.R. Dinglasan, H.Q. Mao, Critical size limit of biodegradable nanoparticles for enhanced lymph node trafficking and paracortex penetration, Nano Res. 12 (2019) 837–844.
[36] A. Schudel, D.M. Francis, S.N. Thomas, Material design for lymph node drug delivery, Nat. Rev. Mater. 4 (2019) 415–428.
[37] J.W. Hickey, J.L. Santos, J.-M. Williford, H.-Q. Mao, Control of polymeric nanoparticle size to improve therapeutic delivery, J. Control. Release 219 (2015) 535–547.
[38] J.L. Santos, Y. Ren, J. Vandermark, M.M. Archang, J.M. Williford, H.W. Liu, J. Lee, T.H. Wang, H.Q. Mao, Continuous production of discrete plasmid DNA-Polycation nanoparticles using flash nanocomplexation, Small 12 (2016) 6214–6222.
[39] Z. He, J.L. Santos, H. Tian, H. Huang, Y. Hu, L. Liu, K.W. Leong, Y. Chen, Q. Mao, Scalable fabrication of size-controlled chitosan nanoparticles for oral delivery of insulin, Biomaterials 130 (2017) 28–41.
[40] H. Tian, Z. He, C. Sun, C. Yang, P. Zhao, L. Liu, K.W. Leong, H.-Q. Mao, Z. Liu, Y. Chen, Uniform core-shell nanoparticles with thiolated hyaluronic acid coating to enhance oral delivery of insulin, Adv. Healthc. Mater. 7 (2018), 1800285.
[41] D. Qiao, L. Liu, Y. Chen, C. Xue, Q. Gao, H.Q. Mao, K.W. Leong, Y. Chen, Potency of a scalable Nanoparticulate subunit vaccine, Nano Lett. 18 (2018) 3007–3016.
[42] Z. He, Y. Hu, T. Nie, H. Tang, J. Zhu, K. Chen, L. Liu, K.W. Leong, Y. Chen, H.-Q. Mao, Size-controlled lipid nanoparticle production using turbulent mixing to enhance oral DNA delivery, Acta Biomater. 81 (2018) 195–207.
[43] Z. He, Z. Liu, H. Tian, Y. Hu, L. Liu, K.W. Leong, H.-Q. Mao, Y. Chen, Scalable production of core-shell nanoparticles by flash nanocomplexation to enhance mucosal transport for oral delivery of insulin, Nanoscale. 10 (2018) 3307–3319.
[44] D. Kumar, N. Saini, N. Jain, R. Sareen, V. Pandit, Gold nanoparticles: an era in bionanotechnology, Expert Opin Drug Deliv. 10 (2013) 397–409.
[45] N.S. Wilson, D. El-Sukkari, G.T. Belz, C.M. Smith, R.J. Steptoe, W.R. Heath, K. Shortman, J.A. Villadangos, Most lymphoid organ dendritic cell types are phenotypically and functionally immature, Blood 102 (2003) 2187–2194.
[46] H. Kobayashi, S. Kawamoto, M. Bernardo, M.W. Brechbiel, M.V. Knopp, P.L. Choyke, Delivery of gadolinium-labeled nanoparticles to the sentinel lymph node: comparison of the sentinel node visualization and estimations of intra-nodal gadolinium concentration by the magnetic resonance imaging, J. Control. Release 111 (2006) 343–351.
[47] O. Lieleg, R.M. Baumgärtel, A.R. Bausch, R.M. Baumgartel, A.R. Bausch, Selective filtering of particles by the extracellular matrix: an electrostatic bandpass, Biophys. J. 97 (2009) 1569–1577.
[48] T. Stylianopoulos, M.Z. Poh, N. Insin, M.G. Bawendi, D. Fukumura, L.L. Munn, R.K. Jain, Diffusion of particles in the extracellular matrix: the effect of repulsive electrostatic interactions, Biophys. J. 99 (2010) 1342–1349.
[49] M.A. Swartz, The physiology of the lymphatic system, Adv. Drug Deliv. Rev. 50 (2001) 3–20.
[50] C.L. Willard-Mack, Normal structure, function, and histology of lymph nodes, Toxicol. Pathol. 34 (2006) 409–424.
[51] J.R. Casley-Smith, The fine structure and functioning of tissue channels and lymphatics, Lymphology 13 (1980) 177–183.
[52] V. Manolova, A. Flace, M. Bauer, K. Schwarz, P. Saudan, M.F. Bachmann, Nanoparticles target distinct dendritic cell populations according to their size, Eur. J. Immunol. 38 (2008) 1404–1413.
[53] C.M. Jewell, S.C. Bustamante Lopez, D.J. Irvine, In situ engineering of the lymph node microenvironment via intranodal injection of adjuvant-releasing polymer particles, Proc. Natl. Acad. Sci. 108 (2011) 15745–15750.
[54] M. Sixt, N. Kanazawa, M. Selg, T. Samson, G. Roos, D.P. Reinhardt, R. Pabst, M.B. Lutz, L. Sorokin, The conduit system transports soluble antigens from the afferent lymph to resident dendritic cells in the T cell area of the lymph node, Immunity 22 (2005) 19–29.
[55] R. Roozendaal, T.R. Mempel, L.A. Pitcher, S.F. Gonzalez, A. Verschoor, R.E. Mebius, U.H. von Andrian, M.C. Carroll, Conduits mediate transport of low-molecular-weight antigen to lymph node follicles, Immunity 30 (2009) 264–276.
[56] M.A. Swartz, J.A. Hubbell, S.T. Reddy, Lymphatic drainage function and its immunological implications: from dendritic cell homing to vaccine design, Semin. Immunol. 20 (2008) 147–156.
[57] K.-H. Chen, D.J. Lundy, E.K. Toh, C.-H. Chen, C. Shih, P. Chen, H.-C. Chang, J.J. Lai, P.S. Stayton, A.S. Hoffman, P.C. Hsieh, Nanoparticle distribution during systemic inflammation is size-dependent and organ-specific, Nanoscale 7 (2015).
[58] M.P. Kai, H.E. Brighton, C.A. Fromen, T.W. Shen, J.C. Luft, Y.E. Luft, A.W. Keeler, G.R. Robbins, J.P.Y. Ting, W.C. Zamboni, J.E. Bear, J.M. DeSimone, Tumor presence induces global immune changes and enhances nanoparticle clearance, ACS Nano 10 (2016) 861–870.

[59] S. Kang, S. Ahn, J. Lee, J.Y. Kim, M. Choi, V. Gujrati, H. Kim, J.Y. Kim, E.C. Shin, S. Jon, Effects of gold nanoparticle-based vaccine size on lymph node delivery and cytotoxic T-lymphocyte responses, J. Control. Release 256 (2017) 56–67.
[60] A. Stano, C. Nembrini, M.A. Swartz, J.A. Hubbell, E. Simeoni, Nanoparticle size influences the magnitude and quality of mucosal immune responses after intranasal immunization, Vaccine 30 (2012) 7541–7546.
[61] Q. Zhou, Y. Zhang, J. Du, Y. Li, Y. Zhou, Q. Fu, J. Zhang, X. Wang, L. Zhan, Different-sized gold nanoparticle activator/antigen increases dendritic cells accumulation in liver-draining lymph nodes and CD8+ T cell responses, ACS Nano 10 (2016) 2678–2692.
[62] C. Guiducci, G. Ott, J.H. Chan, E. Damon, C. Calacsan, T. Matray, K.-D. Lee, R.L. Coffman, F.J. Barrat, Properties regulating the nature of the plasmacytoid dendritic cell response to toll-like receptor 9 activation, J. Exp. Med. 203 (2006) 1999–2008.
[63] S. Chinnathambi, S. Chen, S. Ganesan, N. Hanagata, Binding mode of CpG oligodeoxynucleotides to nanoparticles regulates bifurcated cytokine induction via toll-like receptor 9, Sci. Rep. 2 (2012) 534.
[64] J.A. Leleux, P. Pradhan, K. Roy, Biophysical attributes of CpG presentation control TLR9 signaling to differentially polarize systemic immune responses, Cell Rep. 18 (2017) 700–710.
[65] J. Yue, R.M. Pallares, L.E. Cole, E.E. Coughlin, C.A. Mirkin, A. Lee, T.W. Odom, Smaller CpG-conjugated gold nanoconstructs achieve higher targeting specificity of immune activation, ACS Appl. Mater. Interfaces 10 (2018) 21920–21926.
[66] S. Yan, B.E. Rolfe, B. Zhang, Y.H. Mohammed, W. Gu, Z.P. Xu, Polarized immune responses modulated by layered double hydroxides nanoparticle conjugated with CpG, Biomaterials 35 (2014) 9508–9516.
[67] X. Li, A.M. Aldayel, Z. Cui, Aluminum hydroxide nanoparticles show a stronger vaccine adjuvant activity than traditional aluminum hydroxide microparticles, J. Control. Release 173 (2014) 148–157.
[68] E.J. Park, S.N. Kim, M.S. Kang, B.S. Lee, C. Yoon, U. Jeong, Y. Kim, G.H. Lee, D.W. Kim, J.S. Kim, A higher aspect ratio enhanced bioaccumulation and altered immune responses due to intravenously-injected aluminum oxide nanoparticles, J. Immunotoxicol. 13 (2016) 439–448.
[69] N.P. Truong, M.R. Whittaker, C.W. Mak, T.P. Davis, The importance of nanoparticle shape in cancer drug delivery, Expert Opin. Drug Deliv. 12 (2015) 129–142.
[70] J.-M. Williford, J.L. Santos, R. Shyam, H.-Q. Mao, Shape control in engineering of polymeric nanoparticles for therapeutic delivery, Biomater. Sci. 3 (2015) 894–907.
[71] Y. Geng, P. Dalhaimer, S. Cai, R. Tsai, M. Tewari, T. Minko, D.E. Discher, Shape effects of filaments versus spherical particles in flow and drug delivery, Nat. Nanotechnol. 2 (2007) 249–255.
[72] J.A. Champion, S. Mitragotri, Shape induced inhibition of phagocytosis of polymer particles, Pharm. Res. 26 (2009) 244–249.
[73] J.A. Champion, S. Mitragotri, Role of target geometry in phagocytosis, Proc. Natl. Acad. Sci. 103 (2006) 4930–4934.
[74] P.P. Wibroe, A.C. Anselmo, P.H. Nilsson, A. Sarode, V. Gupta, R. Urbanics, J. Szebeni, A.C. Hunter, S. Mitragotri, T.E. Mollnes, S.M. Moghimi, Bypassing adverse injection reactions to nanoparticles through shape modification and attachment to erythrocytes, Nat. Nanotechnol. 12 (2017) 589–594.
[75] G. Sharma, D.T. Valenta, Y. Altman, S. Harvey, H. Xie, S. Mitragotri, J.W. Smith, Polymer particle shape independently influences binding and internalization by macrophages, J. Control. Release 147 (2010) 408–412.
[76] R. Agarwal, V. Singh, P. Jurney, L. Shi, S.V. Sreenivasan, K. Roy, Mammalian cells preferentially internalize hydrogel nanodiscs over nanorods and use shape-specific uptake mechanisms, Proc. Natl. Acad. Sci. 110 (2013) 17247–17252.
[77] R. Mammadov, G. Cinar, N. Gunduz, M. Goktas, H. Kayhan, S. Tohumeken, A.E. Topal, I. Orujalipoor, T. Delibasi, A. Dana, S. Ide, A.B. Tekinay, M.O. Guler, Virus-like nanostructures for tuning immune response, Sci. Rep. 5 (2015) 1–15.
[78] Z. Li, L. Sun, Y. Zhang, A.P. Dove, R.K. O'Reilly, G. Chen, Shape effect of glyconanoparticles on macrophage cellular uptake and immune response, ACS Macro Lett. 5 (2016) 1059–1064.
[79] S. Kumar, A.C. Anselmo, A. Banerjee, M. Zakrewsky, S. Mitragotri, Shape and size-dependent immune response to antigen-carrying nanoparticles, J. Control. Release 220 ((2015) 141–148.
[80] K. Niikura, T. Matsunaga, T. Suzuki, S. Kobayashi, H. Yamaguchi, Y. Orba, A. Kawaguchi, H. Hasegawa, K. Kajino, T. Ninomiya, K. Ijiro, H. Sawa, Gold nanoparticles as a vaccine platform: influence of size and shape on immunological responses in vitro and in vivo, ACS Nano 7 (2013) 3926–3938.
[81] C.A. Fromen, T.B. Rahhal, G.R. Robbins, M.P. Kai, T.W. Shen, J.C. Luft, J.M. DeSimone, Nanoparticle surface charge impacts distribution, uptake and lymph node trafficking by pulmonary antigen-presenting cells, Nanomedicine 12 (2016) 677–687.
[82] Y. Kakizawa, J.S. Lee, B. Bell, T.M. Fahmy, Precise manipulation of biophysical particle parameters enables control of proinflammatory cytokine production in presence of TLR 3 and 4 ligands, Acta Biomater. 57 (2017) 136–145.
[83] B.S. Doddapaneni, S. Kyryachenko, S.E. Chagani, R.G. Alany, D.A. Rao, A.K. Indra, A.W.G. Alani, A three-drug nanoscale drug delivery system designed for preferential lymphatic uptake for the treatment of metastatic melanoma, J. Control. Release 220 ((2015) 503–514.
[84] Z.G. Yue, W. Wei, P.P. Lv, H. Yue, L.Y. Wang, Z.G. Su, G.H. Ma, Surface charge affects cellular uptake and intracellular trafficking of chitosan-based nanoparticles, Biomacromolecules 12 (2011) 2440–2446.
[85] M.-L. De Temmerman, S.J. Soenen, N. Symens, B. Lucas, R.E. Vandenbroucke, C. Libert, J. Demeester, S.C. De Smedt, U. Himmelreich, J. Rejman, Magnetic layer-by-layer coated particles for efficient MRI of dendritic cells and mesenchymal stem cells, Nanomedicine (London) 9 (2014) 1363–1376.
[86] L.M. Kranz, M. Diken, H. Haas, S. Kreiter, C. Loquai, K.C. Reuter, M. Meng, D. Fritz, F. Vascotto, H. Hefesha, C. Grunwitz, M. Vormehr, Y. Hüsemann, A. Selmi, A.N. Kuhn, J. Buck, E. Derhovanessian, R. Rae, S. Attig, J. Diekmann, R.A. Jabulowsky, S. Heesch, J. Hassel, P. Langguth, S. Grabbe, C. Huber, Ö. Türeci, U. Sahin, Systemic RNA delivery to dendritic cells exploits antiviral defence for cancer immunotherapy, Nature 534 (2016) 396–401.
[87] Y.C. Tseng, Z. Xu, K. Guley, H. Yuan, L. Huang, Lipid-calcium phosphate nanoparticles for delivery to the lymphatic system and SPECT/CT imaging of lymph node metastases, Biomaterials 35 (2014) 4688–4698.
[88] S. Grabbe, H. Haas, M. Diken, L.M. Kranz, P. Langguth, U. Sahin, Translating nanoparticulate-personalized cancer vaccines into clinical applications: case study with RNA-lipoplexes for the treatment of melanoma, Nanomedicine 11 (2016) 2723–2734.
[89] S. Rosigkeit, M. Meng, C. Grunwitz, P. Gomes, A. Kreft, N. Hayduk, R. Heck, G. Pickert, K. Ziegler, Y. Abassi, J. Röder, L. Kaps, F. Vascotto, T. Beissert, S. Witzel, A. Kuhn, M. Diken, D. Schuppan, U. Sahin, H. Haas, E. Bockamp, Monitoring translation activity of mRNA-loaded nanoparticles in mice, Mol. Pharm. 15 (2018) 3909–3919.
[90] V. Kumar, S. Patel, E. Tcyganov, D.I. Gabrilovich, The nature of myeloid-derived suppressor cells in the tumor microenvironment, Trends Immunol. 37 (2016) 208–220.
[91] W. He, P. Liang, G. Guo, Z. Huang, Y. Niu, L. Dong, C. Wang, J. Zhang, Re-polarizing myeloid-derived suppressor cells (MDSCs) with cationic polymers for cancer immunotherapy, Sci. Rep. 6 (2016), 24506.
[92] C. Rosales, Neutrophil: a cell with many roles in inflammation or several cell types? Front. Physiol. 9 (2018) 1–17.
[93] T.L. Hwang, I.A. Aljuffali, C.F. Lin, Y.T. Chang, J.Y. Fang, Cationic additives in nanosystems activate cytotoxicity and inflammatory response of human neutrophils: lipid nanoparticles versus polymeric nanoparticles, Int. J. Nanomedicine 10 (2015) 371–385.
[94] K. Hamad-Schifferli, Exploiting the novel properties of protein coronas: emerging applications in nanomedicine, Nanomedicine (London) 10 (2015) 1663–1674.
[95] D. Docter, D. Westmeier, M. Markiewicz, S. Stolte, S.K. Knauer, R.H. Stauber, The nanoparticle biomolecule corona: lessons learned - challenge accepted? Chem. Soc. Rev. 44 (2015) 6094–6121.
[96] U. Sakulkhu, M. Mahmoudi, L. Maurizi, G. Coullerez, M. Hofmann-Amtenbrink, M. Vries, M. Motazacker, F. Rezaee, H. Hofmann, Significance of surface charge and shell material of superparamagnetic iron oxide nanoparticle (SPION) based core/shell nanoparticles on the composition of the protein corona, Biomater. Sci. 3 (2015) 265–278.
[97] L.K. Petersen, Y. Phanse, A.E. Ramer-Tait, M.J. Wannemuehler, B. Narasimhan, Amphiphilic polyanhydride nanoparticles stabilize bacillus anthracis protective antigen, Mol. Pharm. 9 (2012) 874–882.
[98] F. Shima, T. Akagi, T. Uto, M. Akashi, Manipulating the antigen-specific immune response by the hydrophobicity of amphiphilic poly(gamma-glutamic acid) nanoparticles, Biomaterials 34 (2013) 9709–9716.
[99] F. Shima, T. Akagi, M. Akashi, Effect of hydrophobic side chains in the induction of immune responses by nanoparticle adjuvants consisting of amphiphilic poly (gamma-glutamic acid), Bioconjug. Chem. 26 (2015) 890–898.
[100] F. Shima, T. Akagi, M. Akashi, The role of hydrophobicity in the disruption of erythrocyte membrane by nanoparticles composed of hydrophobically modified poly(gamma-glutamic acid), J. Biomater. Sci. Polym. Ed. 25 (2014) 203–210.
[101] J. Kreuter, E. Liehl, U. Berg, M. Soliva, P.P. Speiser, Influence of hydrophobicity on the adjuvant effect of particulate polymeric adjuvants, Vaccine 6 (1988) 253–256.
[102] D.F. Moyano, M. Goldsmith, D.J. Solfiell, D. Landesman-Milo, O.R. Miranda, D. Peer, V.M. Rotello, Nanoparticle hydrophobicity dictates immune response, J. Am. Chem. Soc. 134 (2012) 3965–3967.
[103] H. Yang, S.Y. Fung, S. Xu, D.P. Sutherland, T.R. Kollmann, M. Liu, S.E. Turvey, Amino acid-dependent attenuation of toll-like receptor signaling by peptide-gold nanoparticle hybrids, ACS Nano 9 (2015) 6774–6784.
[104] J. Singh, S. Pandit, V.W. Bramwell, H.O. Alpar, Diphtheria toxoid loaded poly-(epsilon-caprolactone) nanoparticles as mucosal vaccine delivery systems, Methods 38 (2006) 96–105.
[105] R.S. Raghuvanshi, Y.K. Katare, K. Lalwani, M.M. Ali, O. Singh, A.K. Panda, Improved immune response from biodegradable polymer particles entrapping tetanus toxoid by use of different immunization protocol and adjuvants, Int. J. Pharm. 245 (2002) 109–121.
[106] C. Thomas, A. Rawat, L. Hope-Weeks, F. Ahsan, Aerosolized PLA and PLGA nanoparticles enhance humoral, mucosal and cytokine responses to hepatitis B vaccine, Mol. Pharm. 8 (2011) 405–415.
[107] D.A. Rao, M.L. Forrest, A.W.G. Alani, G.S. Kwon, J.R. Robinson, Biodegradable PLGA based nanoparticles for sustained regional lymphatic drug delivery, J. Pharm. Sci. 99 (2010) 2018–2031.
[108] H. Liu, D.J. Irvine, Guiding principles in the design of molecular bioconjugates for vaccine applications, Bioconjug. Chem. 26 (2015) 791–801.
[109] A.C. Anselmo, M. Zhang, S. Kumar, D.R. Vogus, S. Menegatti, M.E. Helgeson, S. Mitragotri, Elasticity of nanoparticles influences their blood circulation, phagocytosis, endocytosis, and targeting, ACS Nano 9 (2015) 3169–3177.
[110] D. Christensen, M. Henriksen-Lacey, A.T. Kamath, T. Lindenstrøm, K.S. Korsholm, J.P. Christensen, A.F. Rochat, P.H. Lambert, P. Andersen, C.A. Siegrist, Y. Perrie, E.M. Agger, A cationic vaccine adjuvant based on a saturated quaternary ammonium lipid have different in vivo distribution kinetics and display a distinct CD4 T cell-inducing capacity compared to its unsaturated analog, J. Control. Release 160 (2012) 468–476.
[111] R. Palomba, A.L. Palange, I.F. Rizzuti, M. Ferreira, A. Cervadoro, M.G. Barbato, C. Canale, P. Decuzzi, Modulating phagocytic cell sequestration by tailoring nanoconstruct softness, ACS Nano 12 (2018) 1433–1444.

[112] Y. Hui, D. Wibowo, Y. Liu, R. Ran, H.F. Wang, A. Seth, A.P.J. Middelberg, C.X. Zhao, Understanding the effects of nanocapsular mechanical property on passive and active tumor targeting, ACS Nano 12 (2018) 2846–2857.
[113] P.J. Murray, T.A. Wynn, Protective and pathogenic functions of macrophage subsets, Nat. Rev. Immunol. 11 (2011) 723–737.
[114] S. Hamdy, A. Haddadi, R.W. Hung, A. Lavasanifar, Targeting dendritic cells with nano-particulate PLGA cancer vaccine formulations, Adv. Drug Deliv. Rev. 63 (2011) 943–955.
[115] A. Mantovani, F. Marchesi, A. Malesci, L. Laghi, P. Allavena, Tumour-associated macrophages as treatment targets in oncology, Nat. Rev. Clin. Oncol. 14 (2017) 399–416.
[116] M. Song, T. Liu, C. Shi, X. Zhang, X. Chen, Bioconjugated manganese dioxide nanoparticles enhance chemotherapy response by priming tumor-associated macrophages toward M1-like phenotype and attenuating tumor hypoxia, ACS Nano 10 (2016) 633–647.
[117] S.S. Yu, C.M. Lau, W.J. Barham, H.M. Onishko, C.E. Nelson, H. Li, C.A. Smith, F.E. Yull, C.L. Duvall, T.D. Giorgio, Macrophage-specific RNA interference targeting via "click", mannosylated polymeric micelles, Mol. Pharm. 10 (2013) 975–987.
[118] R.A. Ortega, W.J. Barham, B. Kumar, O. Tikhomirov, I.D. McFadden, F.E. Yull, T.D. Giorgio, Biocompatible mannosylated endosomal-escape nanoparticles enhance selective delivery of short nucleotide sequences to tumor associated macrophages, Nanoscale 7 (2015) 500–510.
[119] S. Zhu, M. Niu, H. O'Mary, Z. Cui, Targeting of tumor-associated macrophages made possible by PEG-sheddable, mannose-modified nanoparticles, Mol. Pharm. 10 (2013) 3525–3530.
[120] M. Niu, Y.W. Naguib, A.M. Aldayel, Y.C. Shi, S.D. Hursting, M.A. Hersh, Z. Cui, Biodistribution and in vivo activities of tumor-associated macrophage-targeting nanoparticles incorporated with doxorubicin, Mol. Pharm. 11 (2014) 4425–4436.
[121] M. Niu, S. Valdes, Y.W. Naguib, S.D. Hursting, Z. Cui, Tumor-associated macrophage-mediated targeted therapy of triple-negative breast cancer, Mol. Pharm. 13 (2016) 1833–1842.
[122] N. Mohr, C. Kappel, S. Kramer, M. Bros, S. Grabbe, R. Zentel, Targeting cells of the immune system: mannosylated HPMA-LMA block-copolymer micelles for targeting of dendritic cells, Nanomedicine (London) 11 (2016) 2679–2697.
[123] G.N. Shi, C.N. Zhang, R. Xu, J.F. Niu, H.J. Song, X.Y. Zhang, W.W. Wang, Y.M. Wang, C. Li, X.Q. Wei, D.L. Kong, Enhanced antitumor immunity by targeting dendritic cells with tumor cell lysate-loaded chitosan nanoparticles vaccine, Biomaterials 113 (2017) 191–202.
[124] C. Zhang, G. Shi, J. Zhang, H. Song, J. Niu, S. Shi, P. Huang, Y. Wang, W. Wang, C. Li, D. Kong, Targeted antigen delivery to dendritic cell via functionalized alginate nanoparticles for cancer immunotherapy, J. Control. Release 256 (2017) 170–181.
[125] B. Kang, P. Okwieka, S. Schottler, S. Winzen, J. Langhanki, K. Mohr, T. Opatz, V. Mailander, K. Landfester, F.R. Wurm, Carbohydrate-based nanocarriers exhibiting specific cell targeting with minimum influence from the protein corona, Angew. Chem. Int. Ed. Eng. 54 (2015) 7436–7440.
[126] T.H. Tran, R. Rastogi, J. Shelke, M.M. Amiji, Modulation of macrophage functional polarity towards anti-inflammatory phenotype with plasmid DNA delivery in CD44 targeting hyaluronic acid nanoparticles, Sci. Rep. 5 (2015), 16632.
[127] T.H. Tran, S. Krishnan, M.M. Amiji, MicroRNA-223 induced repolarization of peritoneal macrophages using CD44 targeting hyaluronic acid nanoparticles for anti-inflammatory effects, PLoS One 11 (2016), e0152024.
[128] V.Y. Kosovrasti, L.V. Nechev, M.M. Amiji, Peritoneal macrophage-specific TNF-alpha gene silencing in LPS-induced acute inflammation model using CD44 targeting hyaluronic acid nanoparticles, Mol. Pharm. 13 (2016) 3404–3416.
[129] N.N. Parayath, A. Parikh, M.M. Amiji, Repolarization of tumor-associated macrophages in a genetically engineered nonsmall cell lung Cancer model by intraperitoneal administration of hyaluronic acid-based nanoparticles encapsulating MicroRNA-125b, Nano Lett. 18 (2018) 3571–3579.
[130] T.J. Beldman, M.L. Senders, A. Alaarg, C. Perez-Medina, J. Tang, Y. Zhao, F. Fay, J. Deichmoller, B. Born, E. Desclos, N.N. van der Wel, R.A. Hoebe, F. Kohen, E. Kartvelishvily, M. Neeman, T. Reiner, C. Calcagno, Z.A. Fayad, M.P.J. de Winther, E. Lutgens, W.J.M. Mulder, E. Kluza, Hyaluronan nanoparticles selectively target plaque-associated macrophages and improve plaque stability in atherosclerosis, ACS Nano 11 (2017) 5785–5799.
[131] H. Laroui, E. Viennois, B. Xiao, B.S. Canup, D. Geem, T.L. Denning, D. Merlin, Fab'-bearing siRNA TNFalpha-loaded nanoparticles targeted to colonic macrophages offer an effective therapy for experimental colitis, J. Control. Release 186 (2014) 41–53.
[132] L. Shen, S. Krauthäuser, K. Fischer, D. Hobernik, Y. Abassi, A. Dzionek, A. Nikolaev, N. Voltz, M. Diken, M. Krummen, E. Montermann, I. Tubbe, S. Lorenz, D. Strand, H. Schild, S. Grabbe, M. Bros, Vaccination with trifunctional nanoparticles that address CD8+ dendritic cells inhibits growth of established melanoma, Nanomedicine 11 (2016) 2647–2662.
[133] K. Fytianos, S. Chortarea, L. Rodriguez-Lorenzo, F. Blank, C. von Garnier, A. Petri-Fink, B. Rothen-Rutishauser, Aerosol delivery of functionalized gold nanoparticles target and activate dendritic cells in a 3D lung cellular model, ACS Nano 11 (2017) 375–383.
[134] L.J. Cruz, R.A. Rosalia, J.W. Kleinovink, F. Rueda, C.W.G.M. Löwik, F. Ossendorp, Targeting nanoparticles to CD40, DEC-205 or CD11c molecules on dendritic cells for efficient CD8+ T cell response: a comparative study, J. Control. Release 192 (2014) 209–218.
[135] M. Freeley, A. Long, Advances in siRNA delivery to T-cells: potential clinical applications for inflammatory disease, cancer and infection, Biochem. J. 455 (2013) 133–147.
[136] A.O. Kamphorst, R. Ahmed, CD4 T-cell immunotherapy for chronic viral infections and cancer, Immunotherapy. 5 (2013) 975–987.
[137] T.M. Fahmy, P.M. Fong, J. Park, T. Constable, W.M. Saltzman, Nanosystems for simultaneous imaging and drug delivery to T cells, AAPS J. 9 (2007) E171–E180.
[138] N. Dinauer, S. Balthasar, C. Weber, J. Kreuter, K. Langer, H. von Briesen, Selective targeting of antibody-conjugated nanoparticles to leukemic cells and primary T-lymphocytes, Biomaterials 26 (2005) 5898–5906.
[139] G. Chen, W. Chen, Z. Wu, R. Yuan, H. Li, J. Gao, X. Shuai, MRI-visible polymeric vector bearing CD3 single chain antibody for gene delivery to T cells for immunosuppression, Biomaterials 30 (2009) 1962–1970.
[140] Y.C. Lo, M.A. Edidin, J.D. Powell, Selective activation of antigen-experienced T cells by anti-CD3 constrained on nanoparticles, J. Immunol. 191 (2013) 5107–5114.
[141] C.L. Chen, T.Y. Siow, C.H. Chou, C.H. Lin, M.H. Lin, Y.C. Chen, W.Y. Hsieh, S.J. Wang, C. Chang, Targeted Superparamagnetic Iron oxide nanoparticles for in vivo magnetic resonance imaging of T-cells in rheumatoid arthritis, Mol. Imaging Biol. 19 (2017) 233–244.
[142] M. Bottini, F. D'Annibale, A. Magrini, F. Cerignoli, Y. Arimura, M.I. Dawson, E. Bergamaschi, N. Rosato, A. Bergamaschi, T. Mustelin, Quantum dot-doped silica nanoparticles as probes for targeting of T-lymphocytes, Int. J. Nanomedicine 2 (2007) 227–233.
[143] A.N. Endsley, R.J. Ho, Design and characterization of novel peptide-coated lipid nanoparticles for targeting anti-HIV drug to CD4 expressing cells, AAPS J. 14 (2012) 225–235.
[144] A.N. Endsley, R.J. Ho, Enhanced anti-HIV efficacy of indinavir after inclusion in CD4-targeted lipid nanoparticles, J. Acquir. Immune Defic. Syndr. 61 (2012) 417–424.
[145] S. Ramishetti, R. Kedmi, M. Goldsmith, F. Leonard, A.G. Sprague, B. Godin, M. Gozin, P.R. Cullis, D.M. Dykxhoorn, D. Peer, Systemic gene silencing in primary T lymphocytes using targeted lipid nanoparticles, ACS Nano 9 (2015) 6706–6716.
[146] D. Peer, P. Zhu, C.V. Carman, J. Lieberman, M. Shimaoka, Selective gene silencing in activated leukocytes by targeting siRNAs to the integrin lymphocyte function-associated antigen-1, Proc. Natl. Acad. Sci. U. S. A. 104 (2007) 4095–4100.
[147] D. Peer, J.P. Eun, Y. Morishita, C.V. Carman, M. Shimaoka, Systemic leukocyte-directed siRNA delivery revealing cyclin D1 as an anti-inflammatory target, Science 319 (2008) 627–630.
[148] S.S. Kim, D. Peer, P. Kumar, S. Subramanya, H. Wu, D. Asthana, K. Habiro, Y.G. Yang, N. Manjunath, M. Shimaoka, P. Shankar, RNAi-mediated CCR5 silencing by LFA-1-targeted nanoparticles prevents HIV infection in BLT mice, Mol. Ther. 18 (2010) 370–376.
[149] T. Fernandes Stefanello, A. Szarpak-Jankowska, F. Appaix, B. Louage, L. Hamard, B.G. De Geest, B. Van Der Sanden, C.V. Nakamura, R. Auzély-Velty, Thermoresponsive hyaluronic acid nanogels as hydrophobic drug carrier to macrophages, Acta Biomater. 10 (2014) 4750–4758.
[150] C. Schmidt, The benefits of immunotherapy combinations, Nature 552 (2017) S67–S69.
[151] D. Christensen, E.M. Agger, L.V. Andreasen, D. Kirby, P. Andersen, Y. Perrie, Liposome-based cationic adjuvant formulations (CAF): past, present, and future, J. Liposome Res. 19 (2009) 2–11.
[152] O. Even-Or, S. Samira, E. Rochlin, S. Balasingam, A.J. Mann, R. Lambkin-Williams, J. Spira, I. Goldwaser, R. Ellis, Y. Barenholz, Immunogenicity, protective efficacy and mechanism of novel CCS adjuvanted influenza vaccine, Vaccine 28 (2010) 6527–6541.
[153] A.M. Didierlaurent, B. Laupèze, A. Di Pasquale, N. Hergli, C. Collignon, N. Garçon, Adjuvant system AS01: helping to overcome the challenges of modern vaccines, Expert Rev. Vaccines. 16 (2017) 55–63.
[154] N.L. Berinstein, M. Karkada, M.A. Morse, J.J. Nemunaitis, G. Chatta, H. Kaufman, K. Odunsi, R. Nigam, L. Sammatur, L.D. MacDonald, G.M. Weir, M.M. Stanford, M. Mansour, First-in-man application of a novel therapeutic cancer vaccine formulation with the capacity to induce multi-functional T cell responses in ovarian, breast and prostate cancer patients, J. Transl. Med. 10 (2012) 1–12.
[155] K.D. Brewer, G.M. Weir, I. Dude, C. Davis, C. Parsons, A. Penwell, R. Rajagopalan, L. Sammatur, C.V. Bowen, M.M. Stanford, Unique depot formed by an oil based vaccine facilitates active antigen uptake and provides effective tumour control, J. Biomed. Sci. 25 (2018) 1–12.
[156] N.L. Berinstein, M. Karkada, A.M. Oza, K. Odunsi, J.A. Villella, J.J. Nemunaitis, M.A. Morse, T. Pejovic, J. Bentley, M. Buyse, R. Nigam, G.M. Weir, L.D. MacDonald, T. Quinton, R. Rajagopalan, K. Sharp, A. Penwell, L. Sammatur, T. Burzykowski, M.M. Stanford, M. Mansour, Survivin-targeted immunotherapy drives robust polyfunctional T cell generation and differentiation in advanced ovarian cancer patients, Oncoimmunology 4 (2015).
[157] Z. Khan, A.A. Khan, H. Yadav, G.B.K.S. Prasad, P.S. Bisen, Survivin, a molecular target for therapeutic interventions in squamous cell carcinoma, Cell. Mol. Biol. Lett. 22 (2017) 1–32.
[158] J.M. Langley, L.D. Macdonald, G.M. Weir, D. Mackinnon-Cameron, L. Ye, S. Mcneil, B. Schepens, X. Saelens, M.M. Stanford, S.A. Halperin, A respiratory syncytial virus vaccine based on the small hydrophobic protein ectodomain presented with a novel lipid-based formulation is highly immunogenic and safe in adults: a first-in-humans study, J. Infect. Dis. 218 (2018) 378–387.
[159] C. Butts, A. Maksymiuk, G. Goss, D. Soulières, E. Marshall, Y. Cormier, P.M. Ellis, A. Price, R. Sawhney, F. Beier, M. Falk, N. Murray, Updated survival analysis in patients with stage IIIB or IV non-small-cell lung cancer receiving BLP25 liposome vaccine (L-BLP25): phase IIB randomized, multicenter, open-label trial, J. Cancer Res. Clin. Oncol. 137 (2011) 1337–1342.
[160] C. Butts, R.N. Murray, C. Smith, P. Ellis, K. Jasas, A. Maksymiuk, G. Goss, G. Ely, F. Beier, D. Soulières, A multicenter open-label study to assess the safety of a new

formulation of BLP25 liposome vaccine in patients with unresectable stage III non-small-cell lung cancer, Clin. Lung Cancer. 11 (2010) 391–395.
[161] G.T. Wurz, C.J. Kao, M. Wolf, M.W. DeGregorio, Tecemotide: an antigen-specific cancer immunotherapy, Hum. Vaccines Immunother. 10 (2014) 3383–3393.
[162] H.H. Guan, W. Budzynski, R.R. Koganty, M.J. Krantz, M.A. Reddish, J.A. Rogers, B.M. Longenecker, J. Samuel, Liposomal formulations of synthetic MUC1 peptides: effects of encapsulation versus surface display of peptides on immune responses, Bioconjug. Chem. 9 (1998) 451–458.
[163] T. Gargett, M.N. Abbas, P. Rolan, J.D. Price, K.M. Gosling, A. Ferrante, A. Ruszkiewicz, I.I.C. Atmosukarto, J. Altin, C.R. Parish, M.P. Brown, Phase I trial of Lipovaxin-MM, a novel dendritic cell-targeted liposomal vaccine for malignant melanoma, Cancer Immunol. Immunother. 67 (2018) 1461–1472.